Distributed Joint Power, Association and Flight Control for Massive-MIMO Self-Organizing Flying Drones

Zhangyu Guan, *Member, IEEE*, Nan Cen, *Member, IEEE*,
Tommaso Melodia, *Fellow, IEEE, Senior Member, ACM*, and Scott M. Pudlewski, *Member, IEEE*

***Abstract*— This article studies distributed algorithms to control self-organizing flying drones with massive MIMO networking capabilities - a network scenario referred to as *mDroneNet*. We attempt to answer the following fundamental question: *what is the optimal way to provide spectrally-efficient wireless access to a multitude of ground nodes with mobile hotspots mounted on drones and endowed with a large number of antennas; when we can control the position of the drone hotspots, the association between the ground users and the drone hotspots, as well as the pilot sequence assignment and transmit power for the ground users?* To the best of our knowledge, this is the first time that massive MIMO capabilities are considered in self-organizing flying drone networks. We first derive a mathematical formulation of the problem of joint power, association and movement control in mDroneNet, with the objective of maximizing the aggregate spectral efficiency of the ground users. It is shown that the resulting network control problem is a mixed integer nonlinear nonconvex programming (MINLP) problem. Then, a distributed solution algorithm with polynomial time complexity is designed by solving three closely-coupled subproblems: access association, joint pilot sequence assignment and power control, and drone movement control. As a performance benchmark, a globally-optimal but centralized solution algorithm is also designed based on a combination of the branch and bound framework and convex relaxation techniques. Results indicate that the distributed solution algorithm converges fast (within tens of iterations) and achieves a network spectral efficiency very close to the global optimum obtained by the centralized solution algorithm (over 90% in average).**

***Index Terms*— Wireless Drone Networking, Massive MIMO, Distributed Control, Nonconvex Optimization.**

Manuscript received December 21, 2018; revised July 13, 2019 and December 30, 2019; accepted March 11, 2020; approved by IEEE/ACM TRANSACTIONS ON NETWORKING Editor T. Hou. Date of publication April 29, 2020; date of current version August 18, 2020. This work was supported in part by the Air Force Research Laboratory under Contract FA8750-18-C-0122. This article was presented at the Mediterranean Ad Hoc Networking Workshop (Med-Hoc-Net), Capri, Italy, June 2018. *(Corresponding author: Zhangyu Guan.)*

Zhangyu Guan is with the Department of Electrical Engineering, University at Buffalo, The State University of New York, Buffalo, NY 14260 USA (e-mail: guan@buffalo.edu).

Nan Cen is with the Department of Computer Science, Missouri University of Science and Technology, Rolla, MO 65401 USA (e-mail: nancen@mst.edu).

Tommaso Melodia is with the Institute for the Wireless Internet of Things, Department of Electrical and Computer Engineering, Northeastern University, Boston, MA 02115 USA (e-mail: melodia@ece.neu.edu).

Scott M. Pudlewski is with the Air Force Research Laboratory (AFRL), Rome, NY 13440 USA (e-mail: scott.pudlewski.1@us.af.mil).

Digital Object Identifier 10.1109/TNET.2020.2985972

I. INTRODUCTION

WIRELESS data traffic is drastically increasing following the increased prevalence of video streaming applications and the explosion of the Internet of Things (IoT), such as augmented reality, intelligent transportation and surveillance [2]–[6]. This has resulted in an increasing demand for faster wireless communication networks with higher spectral efficiency, as well as techniques to reduce the interference between co-located wireless links operating on the same spectrum bands and hence to increase the spectral efficiency [7], [8]. In this article, we focus on studying new approaches to provide ground connectivity by exploring the application of self-organizing flying drones (aka unmanned aerial vehicles or UAVs) with massive MIMO networking capabilities, a network scenario we refer to as *mDroneNet*.[1]

mDroneNet. As illustrated in Fig. 1, in mDroneNet there are a set of many-antenna-enabled flying drones to collaboratively provide data collection and forwarding services to a group of single-antenna ground users, and send to the ground users control commands generated either locally at the drones or in a remote fusion center. A wide range of new applications can be enabled by using massive MIMO on UAVs, including high-data-rate mobile multimedia sensing and networking through massive MIMO communications, beamforming-based spectrum sharing and coexistence in the unlicensed spectrum bands with redeployable drone base stations, secure wireless networking in contested environments through massive-MIMO-based directional communications, aerial edge computing with massive-MIMO-enabled flying drones, among others. In this article, we attempt to study the best way to provide spectrally-efficient wireless access to a group of ground users with mobile hotspots mounted on flying drones and endowed with a large number of antennas; when we can control the movement of the drones, access association, as well as the pilot assignment and transmit power for the massive MIMO communications between the ground users and the drones. It is worth pointing out that the operation time of a drone is affected by different factors, including the lifetime of the battery, the energy source type, as well as the weight,

[1]It is reasonable to integrate massive MIMO on UAVs. This is because massive MIMO can achieve realistic form factors as long as different ground users have distinct spatial channel characteristics rather than that the antennas observe uncorrelated channels [9]. As a result, e.g., at 2 GHz frequency band it requires only a 0.75×0.75 meter array to deploy 100 dual-polarized antennas, for which it is practical to deploy the antennas on currently available commercial off-the-shelf UAVs.

speed and flight trajectory of the drone, among others [10]. Recently new technologies have been proposed to extend the battery duration, e.g., automated battery swap and recharge [11], [12] and dynamic recharging scheduling [13], [14].

In mDroneNet these network control strategies are tightly coupled with each other and should therefore be jointly considered to obtain the optimal network operating point. Compared to infrastructure-based cellular networks with static massive MIMO base stations [9], [15]–[18], a peculiar feature of mDroneNet is that the drone hotspots can provide coverage with higher spectral efficiency, by moving dynamically to adapt to the changes in the location or traffic demands of the ground nodes, nodes leaving or joining the network, as well as time and the spatially-varying interference level, among others. Moreover, in mDroneNet a massive MIMO transmission is typically conducted in two phases: pilot-based channel estimation and data transmission, while all the ground nodes are allowed to operate over the entire available spectrum band and at any transmission time. In this setting, the maximum number of ground nodes associated to a drone hotspot is constrained by the length (in symbols) of the pilot sequences used in the channel estimation phase. Pilot contamination will occur if the same pilot sequence is shared by multiple users, and this will result in degraded accuracy of channel estimation and hence lower spectral efficiency [19], [20]. Therefore, it is imperative to jointly regulate the transmit power of the ground nodes as well as the association among the ground nodes, the drone hotspots and the available pilot sequences, to eliminate the mutual interference caused by imperfect channel orthogonalization in the case of limited number antennas at each drone.

Novelty and Contributions. Massive MIMO networking has recently received a significant attention in the scientific literature [9], [15]–[18], [21]–[30]. Readers are referred to [9], [19], [20], [31], [32] and references therein for excellent surveys of the main results in this area. However, most existing research on massive MIMO has been focusing on theoretical analysis of spectral/energy efficiency [15], designing new beamforming signal processing technologies [9], [16], increasing robustness against both unintended interference [17], [18] and one-way/two-way droning [26]–[30] in infrastructure-based cellular networks with static massive-MIMO-enabled base stations, while the potential of massive MIMO in infrastructure-less wireless ad hoc networks has not been explored yet. While unmanned aerial networking has also attracted extensive research in the past decade with a large and growing body of literature [33]–[52], very few of these work has taken massive MIMO into consideration. *To the best of our knowledge, this is for the first time massive MIMO is considered in large-scale wireless networks with self-organizing flying drone hotspots.*

As will be clear in Section III, the resulting mDroneNet control problem studied in this article is a mixed integer nonlinear nonconvex programming (MINLP) problem because of the binary variables for access association and pilot assignment. Such problems are generally NP-hard and there is no existing solution algorithm that can be used to obtain the globally optimal solution with polynomial computational complexity. In this paper, we claim the following main contributions:

- *mDroneNet framework and formulation*. We study for the first time mDroneNet, a new framework for self-organizing aerial drone hotspots with massive MIMO networking capabilities. Our objective is to maximize the spectral efficiency of mDroneNet by jointly controlling the movement of the drones, access association and pilot assignment, as well as the transmit power of the ground users.
- *Distributed solution algorithms.* As in [53], we focus on distributed algorithm design for mDroneNet. Compared to centralized control, distributed control does not require the network to collect the full statistical channel state information (CSI), the power of noise and locations, among other network parameters, from all the ground users and flying UAVs at a centralized control entity. As a result, the network control does not suffer from the single point of failure problem and hence is more robust. Moreover, distributed algorithms are essential particularly in large-scale wireless networks with multiple self-organizing UAVs and ground users for scalable and low-latency network control. In this work, we decompose the resulting MINLP problem into three distributed subproblems based on primal decomposition, and design solution algorithms for each of them: user-drone access association, joint pilot assignment and power control, and drone movement control.
- *Globally optimal solution algorithm.* To provide a performance benchmark for the distributed solution algorithm, we design a centralized but globally optimal solution algorithm based on *a combination of the branch and bound framework and of convex relaxation techniques* that can result in an ε-optimal solution with ε being a predefined level of optimality precision.
- *Performance evaluation.* The performance of the proposed distributed solution algorithm is evaluated in terms of network spectral efficiency by comparing it to the global optimum through extensive simulation experiments. Results indicate that the distributed solution algorithm can achieve on average over 90% of the global optimum. The convergence behaviors of the proposed solution algorithms are also evaluated.

The remainder of the paper is organized as follows. We review related work in Section II, and describe the system model and problem formulation in Section III. In Sections IV and V, we present the distributed solution algorithm and the centralized solution algorithm, respectively. Performance evaluation of the proposed solution algorithms is presented in Section VI, and finally we draw conclusions in Section VII.

II. Related Work

There is a large and growing body of literature on unmanned aerial vehicular networking, focusing on UAV-assisted guidance [33], UAV-based data collection [34], [37], [38] and relaying [35], [36], [39], [41], [43], [45], [46], ground-aerial channel measurements [40] as well as tracking and control of UAV networks [42], [44], [54]. Readers are referred to [47]–[52] and references therein for an extensive survey of this research area. Most of these works focus on single-antenna aerial vehicles and conventional MIMO, with very few recent efforts considering massive MIMO [54]. Different from [54], where Chandhar *et al.* derived the achievable uplink capacity from a many-antenna ground base station to a set of single-antenna aerial drones, in this paper we maximize the aggregate throughput of single-antenna ground nodes served by a set of aerial drones each endowed with a large number of antennas.

Compared to conventional multiuser MIMO, massive MIMO can attain much higher spectral efficiency by using a

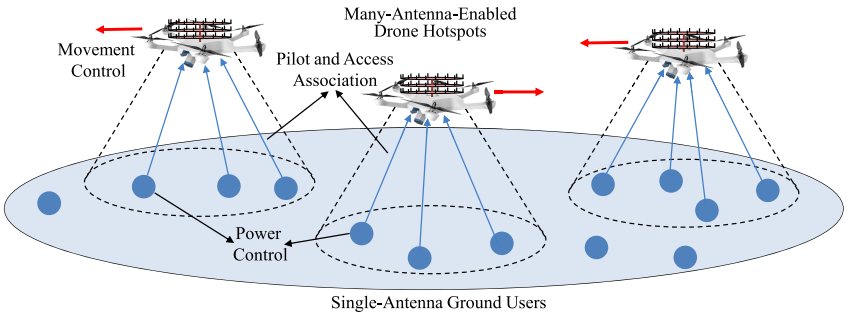

Fig. 1. mDroneNet: Wireless networks with massive-MIMO self-organizing flying UAVs.

large number of antennas with low-complexity linear precoding technologies [16], [19], [27]–[30], [55]. In [29], the authors derived an exact achievable rate expression in closed-form for maximum-ratio combining/maximum-ratio transmission (MRC/MRT) processing and an analytical approximation of the achievable rate for zero-forcing (ZF) processing for multi-pair full-duplex massive MIMO relay system. In [27], Jin *et al.* derived the ergodic rates in the case of a finite number of antennas and concluded that the ergodic sum-rate can be maintained while the relay power is scaled down by a factor of the number of the antennas at the relay over the number of users. Amarasuriya investigated in [28] multi-user massive MIMO relay networks with ZF-processing by deriving the achievable sum rate expressions in both perfect and imperfect CSI cases. In [55], the problem of joint power and time allocation is addressed for secure communications in a decode-and-forward massive MIMO relaying system in the presence of adversary eavesdroppers. In [30], the spectral and energy efficiency for multiple amplify-and-forward two-way full-duplex massive MIMO relay systems are studied. Finally, [9], [19], [20], [31], [32] contain good surveys and tutorials on massive MIMO networking. These papers are focused on infrastructure-based cellular networks with static many-antenna-enabled base stations, and focus on asymptotic performance analysis with respect to a single network parameter (e.g., power). Our paper, instead, considers for the first time aerial drone hotspots with massive MIMO capabilities in infrastructure-less network scenarios.[2]

III. System Model and Problem Statement

We consider wireless networks where a set of many-antenna drone hotspots serve a set of single-antenna ground users, as illustrated in Fig. 1. The drones collect field information from the users, make action decisions either locally at each drone or by sending the information fusion results to a remote control center, and finally send the action commands back to the ground users. Our objective is to maximize the network-wide spectral efficiency for the uplink transmissions since it causes only low-level traffic load to transmit information fusion results and control commands in the downlinks. We consider joint control of the movement of aerial drones, the association among the ground users and the drones, as well as the pilot sequence assignment and transmit power control for the ground nodes. It is worth pointing out that we consider single-antenna ground users in mDroneNet because we want to keep the theoretical analysis and algorithm design tractable, while the control of mDroneNet with multiple-antenna ground users will be studied in our future research. Next, we formalize the network control problem by describing the system model. The key notations are summarized in Table I for the reader's convenience.

[2]Each drone hotspot is essentially a mobile base station and can serve as the mobile infrastructure for ground wireless networks. In this paper by infrastructure-less networks we refer to wireless networks without centralized coordination of the self-organizing flying hotspots.

TABLE I
Summary of Key Notations

Notation	Physical Meaning
$\mathcal{A}$	Set of all aerial drones
$\mathcal{G}$	Set of all ground users
$\mathcal{G}_a$	Set of ground users associated to drone $a \in \mathcal{A}$
$\mathcal{W}$	Set of pilot sequences available to mDroneNet
α_{ga}	1 if ground user g is associated to drone a, and 0 otherwise
$\boldsymbol{\alpha}$	Access association vector: $(\alpha_{ga})_{g\in\mathcal{G}}^{a\in\mathcal{A}}$
p_g	Transmit power of ground user $g \in \mathcal{G}$
$\mathbf{p}$	Transmit power vector of ground nodes: $(p_g)_{g\in\mathcal{G}}$
μ_{gw}	1 if pilot sequence $w \in \mathcal{W}$ is used by ground user g, and 0 otherwise
$\boldsymbol{\mu}$	Pilot sequence assignment vector: $(\mu_{gw})_{g\in\mathcal{G}}^{w\in\mathcal{W}}$
x_a, y_a, z_a	x-, y- and z-axis coordinates of drone $a \in \mathcal{A}$
$\mathbf{x}, \mathbf{y}, \mathbf{z}$	x-, y- and z-axis coordinate vector of drones: $(x_a)_{a\in\mathcal{A}}$, $(y_a)_{a\in\mathcal{A}}$, and $(z_a)_{a\in\mathcal{A}}$
$p_{\max}$	Maximum transmit power of ground node
γ_g	Achievable SINR of ground node $g \in \mathcal{G}$
τ	Pilot sequence length in symbol
M	The number of antennas of each drone hotspot
$a(g)$	Service aerial drone of node $g \in \mathcal{G}$
$\beta_{g'g}$	Channel gain from ground node g' to aerial drone $a(g)$
$\mathcal{I}_g$	The set of ground users sharing the same pilot sequence with user g
$\mathcal{A}(\mathcal{I}_g)$	Set of aerial drones of interfering nodes in $\mathcal{I}_g$
$H_{g'g}$	Path loss from ground node g' to aerial drone $a(g)$
ρ_g	Nominal SNR for ground user g
G_a	The number of ground users served by drone $a \in \mathcal{A}$
$G_{\max}$	Maximum of G_a
R_g	Achievable throughput of ground node $g \in \mathcal{G}$

System Model. As mentioned in Section I, a massive MIMO transmission is typically accomplished in two phases, i.e., channel estimation and data transmission [19], [20], [31]. In our case, the ground users send a set of pilot sequences to the drones for channel estimation in the first phase, while in the second phase the drones detect the data from the users based on the estimated channel state information (CSI). Denote $\mathcal{A}$, $\mathcal{G}$ and $\mathcal{W}$ as the sets of the drone hotspots, ground users, and the available pilot sequences, respectively. Define α_{ga} as the access association variable. Let $\alpha_{ga} = 1$ if user $g \in \mathcal{G}$ is associated with drone $a \in \mathcal{A}$, and $\alpha_{ga} = 0$ otherwise. Denote the access association vector as $\boldsymbol{\alpha} \triangleq (\alpha_{ga})_{g\in\mathcal{G}}^{a\in\mathcal{A}}$. Similarly, let $\boldsymbol{\mu} = (\mu_{gw})_{g\in\mathcal{G}}^{w\in\mathcal{W}}$ represent the pilot sequence allocation

vector, with $\mu_{gw} = 1$ if pilot sequence is associated to ground user g and $\mu_{gw} = 0$ otherwise. We consider single-home accommodation for the ground users in favor of tractable complexity in modeling and theoretical analysis, i.e., each ground user is associated to at most one drone hotspot and at most one pilot sequence. Then we have

$$\alpha_{ga} \in \{0,\ 1\}, \quad \forall g \in \mathcal{G},\ a \in \mathcal{A} \tag{1}$$

$$\mu_{gw} \in \{0,\ 1\}, \quad \forall g \in \mathcal{G},\ w \in \mathcal{W} \tag{2}$$

$$\sum_{a \in \mathcal{A}} \alpha_{ga} \leq 1, \quad \forall g \in \mathcal{G}, \tag{3}$$

$$\sum_{g \in \mathcal{G}} \alpha_{ga} \leq G_{\max}, \quad \forall a \in \mathcal{A}, \tag{4}$$

$$\sum_{w \in \mathcal{W}} \mu_{gw} \leq 1, \quad \forall g \in \mathcal{G}, \tag{5}$$

where $G_{\max}$ is the maximum number of ground users that can be served by each drone hotspot $a \in \mathcal{A}$.[3] Let $\mathcal{G}_a \subset \mathcal{G}$ and $\mathcal{G}'_w \subset \mathcal{G}$ represent the set of users associated with drone a and the set of users sharing the same pilot sequence w, respectively, i.e., $\mathcal{G}_a \triangleq \{g|\ g \in \mathcal{G},\ \alpha_{ga} = 1\}$ for each $a \in \mathcal{A}$, and $\mathcal{G}'_w \triangleq \{g|\ g \in \mathcal{G},\ \mu_{gw} = 1\}$ for each $w \in \mathcal{W}$. Denote $w(g)$ as the pilot sequence used by ground user g, and let $\mathcal{I}_g(\boldsymbol{\mu}) \triangleq \mathcal{G}'_{w(g)}$ represent the set of users using the same pilot sequence as user g. Similarly, denote $a(g)$ as the service drone of ground user $g \in \mathcal{G}$.

Let x_a, y_a and z_a represent respectively the x-, y- and z-axis coordinates of drone a, and define the coordinate vector for the drones in $\mathcal{A}$ as $\mathbf{x} = (x_a)_{a \in \mathcal{A}}$, $\mathbf{y} = (y_a)_{a \in \mathcal{A}}$ and $\mathbf{z} = (z_a)_{a \in \mathcal{A}}$. Then, the distance between user g' and the service drone of user g (i.e., drone $a(g)$), denoted as $d_{g'g}$, can be expressed as

$$\begin{aligned} d_{g'g} &\triangleq d_{g'g}(x_{a(g)}, y_{a(g)}, z_{a(g)}) \\ &= \sqrt{(x_{a(g)} - \widetilde{x}_{g'})^2 + (y_{a(g)} - \widetilde{y}_{g'})^2 + (z_{a(g)} - \widetilde{z}_{g'})^2}, \end{aligned} \tag{6}$$

where $\widetilde{x}_{g'}$, $\widetilde{y}_{g'}$ and $\widetilde{z}_{g'}$ represent the x-, y- and z-axis coordinates of ground user $g' \in \mathcal{G}$, respectively. Further denote $\beta_{g'g}$ as the channel gain between ground user $g' \in \mathcal{G}$ and drone $a(g)$ (i.e., the service drone of user g). Then $\beta_{g'g}$ can be expressed as $\beta_{g'g} = H_{g'g}\zeta_{g'g}$, where $\zeta_{g'g}$ represents the log-normal slow fading between user g' and drone $a(g)$, $H_{g'g} \triangleq d_{g'g}^{-\chi}$ is location-dependent path loss with χ being path loss factor and the distance $d_{g'g}$ defined in (6).

In this work we focus on the applications of UAVs in networking environments in rich-scattering environments with dense and high blockage, while UAV networking in other scenarios [9], [37], [54], [56]–[58], e.g., LoS-dominant wireless environments, will be studied in our future work. In this setting, we consider a model similar to [59], [60] to express the effective SINR achievable by uplink massive MIMO communication links, which jointly considers the effects of pilot contamination and mutual interference among the ground users. Then, a lower bound of the link capacity achievable by ground user g in the data transmission phase, denoted as C_g, can be represented as

$$C_g = B \log_2(1 + \gamma_g), \tag{7}$$

with γ_g being a lower bound of the effective SINR achievable by ground user $g \in \mathcal{G}$ given as in (8), as shown at the bottom of this page,[4] where τ is the length (in symbols) of each pilot sequence, M represents the number of antennas available at each aerial drone, ρ_g is nominal transmit signal-to-noise ratio (SNR) at ground user g; $|\mathcal{G}_{a(g)}(\boldsymbol{\alpha})|$ is the cardinality of $\mathcal{G}_{a(g)}(\boldsymbol{\alpha})$, i.e., the set of ground users served by the service drone of user g; and finally

$$\xi_{g'g} \triangleq \sum_{l \in \mathcal{I}_{g'}(\boldsymbol{\mu})} \rho_l \beta_{lg} \tag{9}$$

and $\phi_{g'g}$ is defined as

$$\phi_{g'g} = \begin{cases} \beta_{g'g}, & \text{if } a(g') \notin \mathcal{A}(\mathcal{I}_g(\boldsymbol{\mu})) \\ \beta_{g'g}\left(1 - \dfrac{\tau \rho_{g'} \beta_{g'g}}{1 + \tau \xi_{g'g}}\right), & \text{otherwise,} \end{cases} \tag{10}$$

with $\mathcal{A}(\mathcal{I}_g(\boldsymbol{\mu})) \triangleq \{a(g')|g' \in \mathcal{I}_g(\boldsymbol{\mu})\}$ representing the set of service drones of the ground users in $\mathcal{I}_g(\boldsymbol{\mu})$, i.e., the users sharing the same pilot sequence with user g. The average rate achievable in the channel estimation and data transmission phases, denoted as R_g, can then be expressed as $R_g = (1 - \frac{\tau}{T})C_g$, where C_g is the link capacity achievable in the data transmission phase in (7), and τ and T are the length of pilot sequences and the period of a massive MIMO transmission in symbols, respectively [61]. In this work, we design distributed control algorithms for mDroneNet by considering data-transmission-phase link capacity (7) and fixed length of pilot sequences in channel estimation phase.

Problem Statement. Our objective is to maximize the aggregate capacity of all the ground users in $\mathcal{G}$ and hence the network spectral efficiency of the mDroneNet, by jointly determining the access association vector $\boldsymbol{\alpha}$, pilot sequence assignment vector $\boldsymbol{\mu}$, the location vectors $\mathbf{x}$, $\mathbf{y}$ and $\mathbf{z}$ for the

[3]The maximum number of served ground nodes cannot exceed the number of antennas available to each aerial drone and the length of pilot sequences used in channel estimation [15].

[4]It is worth pointing out that we do not assume perfect CSI in this paper. This is because the SINR model accounts for different practical factors that affect massive MIMO networks, including channel-estimation error, the type of linear spatial multiplexing/de-multiplexing, power control, noncoherent inter-cell interference, and coherent inter-cell interference due to pilot contamination, among others [59], [60]. In this setting, as pointed out in [60], (8) provides a lower bound on the achievable SINR while deriving the exact closed-form expression of the achievable SINR is still an open problem as of today. In this work, we study the distributed joint power, association and flight control in self-organizing massive-MIMO drone networks taking this SINR model as an example, while the resulting network control framework is not restricted to any specific SINR models.

$$\gamma_g \triangleq \gamma_g(\boldsymbol{\alpha},\ \boldsymbol{\mu},\ \mathbf{p},\ \boldsymbol{x},\ \boldsymbol{y},\ \boldsymbol{z}) = \frac{\left(M - |\mathcal{G}_{a(g)}(\boldsymbol{\alpha})|\right)\tau \rho_g \beta_{gg}^2(\boldsymbol{x},\ \boldsymbol{y},\ \boldsymbol{z}) p_g / (1 + \tau \xi_{gg})}{1 + \sum\limits_{g' \in \mathcal{G}} \phi_{g'g} p_{g'} + \dfrac{\tau\left(M - |\mathcal{G}_{a(g)}(\boldsymbol{\alpha})|\right) \sum\limits_{g' \in \mathcal{I}_g(\boldsymbol{\mu}) \setminus g} \rho_{g'} \beta_{g'g}^2(\boldsymbol{x},\ \boldsymbol{y},\ \boldsymbol{z}) p_{g'}}{1 + \tau \xi_{gg}}} \tag{8}$$

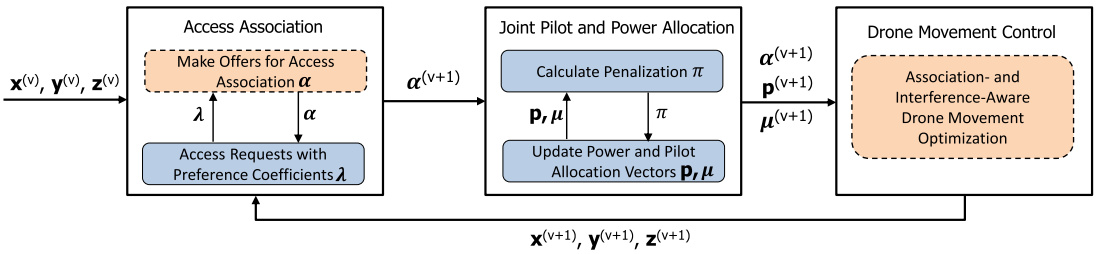

Fig. 2. Diagram of the distributed solution algorithm. The shaded blocks with dashed border represent operations of the drone hotspots while blocks with solid border for the ground users.

drones, as well as the transmit power vector $\mathbf{p}$. The problem is formalized in Problem 1 as follows.

Problem 1

$$\begin{aligned}
&\text{Given}: \ \mathcal{A},\ \mathcal{G}, G_{\max}, M, \widetilde{\mathbf{x}}, \widetilde{\mathbf{y}}, \widetilde{\mathbf{z}}\\
&\underset{\boldsymbol{\alpha},\boldsymbol{\mu},\mathbf{p},\mathbf{x},\mathbf{y},\mathbf{z}}{\text{Maximize}}: \ U \triangleq \sum_{g\in\mathcal{G}} C_g(\boldsymbol{\alpha},\boldsymbol{\mu},\mathbf{p},\mathbf{x},\mathbf{y},\mathbf{z})\\
&\text{Subject to}: \ 0 \le p_g \le p_{\max}, \quad \forall g \in \mathcal{G},\\
&\qquad\qquad x_{\min} \le x_a \le x_{\max}, \ \forall a \in \mathcal{A},\\
&\qquad\qquad y_{\min} \le y_a \le y_{\max}, \ \forall a \in \mathcal{A},\\
&\qquad\qquad z_{\min} \le z_a \le z_{\max}, \ \forall a \in \mathcal{A},\\
&\qquad\qquad Constraints\ (1),\ (2),\ (3),\ (4),\ (5) \qquad (11)
\end{aligned}$$

where $\widetilde{\mathbf{x}}, \widetilde{\mathbf{y}}$ and $\widetilde{\mathbf{z}}$ are the location vectors of the ground users; $C_g(\boldsymbol{\alpha},\boldsymbol{\mu},\mathbf{p},\mathbf{x},\mathbf{y},\mathbf{z}) = C_g$, the objective function of user g, is the lower bound of the rate achievable by the user, as defined through (7)-(10); $p_{\max}$ is the maximum transmit power of each of the ground users in $\mathcal{G}$; and finally $[x_{\min}\ x_{\max}]$ represent the x-axis movement range of the drones while $[y_{\min}\ y_{\max}]$ and $[z_{\min}\ z_{\max}]$ are the ranges of the y- and z-axis, respectively.

The utility function U in (11) is a nonlinear nonconcave function with respect to the control variables because of the complicated mathematical expression of the effective SINR in (8). Moreover, Problem 1 in (11) is a mixed integer-continuous programming problem because of the binary access association variables $\boldsymbol{\alpha}$ and pilot assignment variables $\boldsymbol{\mu}$. Given an arbitrary such problem, there is in general no existing solution algorithm that can be used to obtain the global optimum in polynomial computational complexity. Next, we first present in Section IV a distributed solution algorithm that can be used to achieve a sub-optimal solution to provide a lower-bound on the utility function U in (11). Then in Section V we will design a centralized solution algorithm to provide a performance benchmark for the distributed solution algorithm.

IV. Distributed Solution Algorithm

A key step of the distributed solution algorithm design is to decompose the original network control problem into a series of subproblems, by solving which in a distributed manner the original problem can be solved [62], [63]. However, in our case the control variables $\boldsymbol{\alpha}, \boldsymbol{\mu}, \mathbf{p}, \mathbf{x}, \mathbf{y}$ and $\mathbf{z}$ are closely coupled with each other in the complicated mathematical expression of the effective SINR in (8). As a result, the network control problem, i.e., Problem 1 in (11), is architecturally indecomposable.[5] In this work, the distributed solution algorithms are designed by decomposing the network control problem following a primal decomposition approach. Roughly speaking, with primal decomposition Problem 1 in (11) is solved by dividing the feasible set of the original problem into multiple parts by fixing a subset of variables at a time, which are drone location variables $\mathbf{x}, \mathbf{y}$ and $\mathbf{z}$, association variables $\boldsymbol{\alpha}$ as well as transmit power vector $\mathbf{p}$ and pilot sequence assignment variables $\boldsymbol{\mu}$. The overall diagram of the algorithm design is illustrated in Fig. 2, where the original problem is solved by iteratively solving three subproblems obtained from primal decomposition, i.e., access association, joint pilot assignment and power control, and movement control for the drones.

[5]A problem is architecturally decomposable if its dual problem obtained by introducing Lagrange multipliers can be rewritten into a set of subproblems, each of which can be solved locally in a single protocol layer and network device [62].

A. Access Association

The core idea of the proposed access association strategy is to let the ground users in $\mathcal{G}$ interact iteratively with the drone hotspots in $\mathcal{A}$ to compete for association opportunities based on certain locally-calculated preference criterion, as illustrated in Fig. 2. To this end, in each iteration the ground users first report their own association preferences to the drones, which then make association offers based on the received preference information. Let $\mathbf{x}^{(\nu)}$, $\mathbf{y}^{(\nu)}$ and $\mathbf{z}^{(\nu)}$ represent the coordinates of the drones in current iteration ν. Then in iteration $\nu+1$ the objective of the access association is to maximize the aggregate capacity of all the ground users in $\mathcal{A}$ by determining the association vector $\boldsymbol{\alpha}^{(\nu+1)}$ subject to association constraints (1), (3) and (4).

Denote $\mathcal{A}_g^{(\nu)} \subset \mathcal{A}$ as the set of drones nearby ground user $g \in \mathcal{G}$ (i.e., the drones in the communication range of the ground user). Then, the association preference of ground node g with respect to drone $a \in \mathcal{A}_g^{(\nu)}$, denoted as λ_{ga}, can be computed as

$$\lambda_{ga} = \frac{\log(1+\gamma_{ga})}{\sum\limits_{a'\in\mathcal{A}_g^{(\nu)}} \log(1+\gamma_{ga'})}, \qquad (12)$$

where $\gamma_{ga'}$ represents the interference-free single-input-single-output (SISO) SINR, i.e., the SINR achievable with single antenna and without interference from the other ground users co-located in the mDroneNet, achievable by ground user g if the user is associated with drone $a' \in \mathcal{A}_g^{(\nu)}$. In this work, the SINR $\gamma_{ga'}$ is defined as

$$\gamma_{ga'} \triangleq \rho_g \beta_{gg}|_{a(g)=a'}, \qquad (13)$$

with ρ_g being the transmit SNR for ground user g and $\beta_{gg}|_{a(g)=a'}$ being the path loss for the wireless channel between ground user g and its service drone $a(g)$. Denote $\boldsymbol{\lambda}_a = (\lambda_{ga})_{g\in\widetilde{\mathcal{G}}_a}$ as the preference vector drone a receives

from its nearby ground users in $\widetilde{\mathcal{G}}_a \triangleq \{g | g \in \mathcal{G}, a \in \mathcal{A}_g^{(\nu)}\}$. Then, each drone $a \in \mathcal{A}_g^{(\nu)}$ first sorts $\boldsymbol{\lambda}_a$ in a descending order and then sends association offers to a preferred set of maximum $G_{\max}$ of ground users, as follows,

$$\boldsymbol{\lambda}_a^{\mathrm{dsc}} = (\underbrace{\lambda_{g_1 a}, \lambda_{g_2 a}, \cdots, \lambda_{g_{G_{\max}} a}}_{Preferred\ Ground\ Users}, \cdots), \tag{14}$$

where $G_{\max}$ is the maximum number of users each drone can serve at the same time. Let $\mathcal{A}_g^{\mathrm{offer}}$ represent the subset of the drones that send an association offer to ground user g, and denote $|\mathcal{A}_g^{\mathrm{offer}}|$ as the cardinality of $\mathcal{A}_g^{\mathrm{offer}}$. Then, each user accepts the association offer it receives from the drones corresponding to the highest SISO SINR, i.e., associate with drone a^* with

$$a^* \triangleq \underset{a \in \mathcal{A}_g^{\mathrm{offer}}}{\arg\max}\ \lambda_{ga}, \tag{15}$$

where λ_{ga} is the association preference defined in (12). The above procedure is executed until no ground user receives more than one association offer. The output of this step is the updated access association strategies, i.e., $\boldsymbol{\alpha}^{(\nu+1)}$. The association strategy is summarized in Algorithm 1.

Remark 1: In the association strategy described in Algorithm 1, the rationale of computing the association preference as in (13), i.e., based on the interference-free SISO SINR, is as follows. In massive MIMO settings, particularly when the number of antennas M is large, the received SINR is dominated by the power of noise and large-scale fading effects, e.g., path loss, shadow fading. Therefore, the capacity with interference-free SISO capacity, i.e., (12), can serve as a good indication of association preference and can be computed with low computational complexity.

Algorithm 1 Competition-Based Access Association

Data: Drone coordinates $\mathbf{x}^{(\nu)}$, $\mathbf{y}^{(\nu)}$ and $\mathbf{z}^{(\nu)}$
Result: Updated association vector $\boldsymbol{\alpha}^{(\nu+1)}$
Initialization: Set $|\mathcal{A}_g^{\mathrm{offer}}| = |\mathcal{A}|$, $\forall g \in \mathcal{G}$;
Operations for Ground Users:
while $\exists g \in \mathcal{G}$, $|\mathcal{A}_g^{\mathrm{offer}}| > 1$ **do**
  for *each user* $g \in \mathcal{G}$ **do**
    if $|\mathcal{A}_g^{\mathrm{offer}}| \leq 1$ **then**
      continue;
    else
      for each drone $a \in \mathcal{A}_g$, calculate association preference λ_{ga} based on (12) and (13);
      broadcast the calculated λ_{ga};
    end
    accept association offers based on (15);
    update $\boldsymbol{\alpha}^{(\nu+1)}$;
  end
end
Operations for Drones:
for *each drone* $a \in \mathcal{A}$ **do**
  make association offers based on (14);
end

B. Joint Pilot Assignment and Power Control

With given coordinates of the drones and the updated access association vector, i.e., $\boldsymbol{\alpha}^{(\nu+1)}$ obtained in Section IV-A, as shown in Fig. 2, the objective in the second network control subproblem is to jointly determine the pilot assignment and transmit power for the ground users. The subproblem can be formalized as

$$\begin{aligned} &\textbf{Problem 2} \\ &\text{Given}: \ \mathbf{x}^{(\nu)}, \mathbf{y}^{(\nu)}, \mathbf{z}^{(\nu)}, \boldsymbol{\alpha}^{(\nu+1)} \\ &\underset{\boldsymbol{\mu},\, \mathbf{p}}{\text{Maximize}}: \ U \triangleq \sum_{g \in \mathcal{G}} C_g(\boldsymbol{\mu},\, \mathbf{p}) \\ &\text{Subject to}: \ 0 \leq p_g \leq p_{\max}, \quad \forall g \in \mathcal{G}, \\ &\qquad\qquad Constraints\ (2), (5). \end{aligned} \tag{16}$$

As discussed in Section III, Problem 2 in (16) is a mixed integer nonlinear and nonconvex programming (MINLP) problem because of the complicated mathematical expression of the effective SINR $\gamma_g(\boldsymbol{\mu},\ \mathbf{p})$ in (8) and that the pilot sequence assignment variables take only binary values. Such problems are generally NP-hard and there is typically no existing solution algorithm than can be used to obtain the global optimum in polynomial computational complexity. In this section, we solve Problem 2 by designing a pricing-based distributed solution algorithm. To this end, we first reformulate Problem 2 by relaxing the binary pilot sequence assignment variables $\boldsymbol{\mu}$.

Problem Reformulation. We first relax the pilot sequence assignment variables $\boldsymbol{\mu}$ by allowing each ground user to use multiple pilot sequences. For this purpose, let p_{gw} represent the transmit power that ground user $g \in \mathcal{G}$ allocates to pilot sequence $w \in \mathcal{W}$ and define $\widetilde{\mathbf{p}} = (p_{gw})_{g \in \mathcal{G}}^{w \in \mathcal{W}}$. Then the power constraints in (16) can be rewritten as

$$0 \leq p_{gw} \leq p_{\max}, \quad \forall g \in \mathcal{G}, w \in \mathcal{W}\ , \tag{17}$$

$$\sum_{w \in \mathcal{W}} p_{gw} \leq p_{\max}, \quad \forall g \in \mathcal{G}. \tag{18}$$

$$\gamma_{gw}(\widetilde{\mathbf{p}}) = \frac{\left(M - |\mathcal{G}_{a(g)}|\right) \tau \rho_g \beta_{gg}^2 p_{gw} / (1 + \tau \xi_{gg})}{1 + \sum\limits_{g' \in \mathcal{G}} \sum\limits_{w' \in \mathcal{W}} \mu_{g'g}(\boldsymbol{\mu}) p_{g'w'} + \frac{\tau \left(M - |\mathcal{G}_{a(g)}|\right) \sum\limits_{g' \in \mathcal{I}_g \setminus g} \sum\limits_{w' \in \mathcal{W}} \rho_{g'} \beta_{g'g}^2 p_{g'w'}}{1 + \tau \xi_{gg}}} \tag{19}$$

$$= \frac{\left(M - |\mathcal{G}_{a(g)}|\right) \tau \rho_g \beta_{gg}^2 p_{gw}}{(1 + \tau \xi_{gg})(1 + \sum\limits_{g' \in \mathcal{G}} \sum\limits_{w' \in \mathcal{W}} \mu_{g'g}(\boldsymbol{\mu}) p_{g'w'}) + \tau \left(M - |\mathcal{G}_{a(g)}|\right) \sum\limits_{g' \in \mathcal{I}_g \setminus g} \sum\limits_{w' \in \mathcal{W}} \rho_{g'} \beta_{g'g}^2 p_{g'w}} \tag{20}$$

Algorithm 2 Pricing-Based Joint Pilot and Power Control

Data: Drone coordinates $\mathbf{x}$, $\mathbf{y}$, $\mathbf{z}$; association strategy $\boldsymbol{\alpha}$; $\nu = 0$; current transmit power vector $\widetilde{\mathbf{p}}^{(\nu)}$; $\eta^{(\nu)} > 0$

Result: Updated transmit power $\widetilde{\mathbf{p}}^{(\nu+1)}$;

for *each user* $g \in \mathcal{G}$ **do**
  Compute $\widehat{\mathbf{p}}_g$ by solving Problem 2 (penal) in (27);
  Set $\widetilde{\mathbf{p}}_g^{(\nu+1)} = \widetilde{\mathbf{p}}_g^{(\nu)} + \eta^{(\nu)}(\widehat{\mathbf{p}}_g - \widetilde{\mathbf{p}}_g^{(\nu+1)})$;
end
if $\widetilde{\mathbf{p}}^{(\nu+1)}$ *satisfies certain termination criterion* **then**
  STOP;
else
  Set $\nu = \nu + 1$; go to Step 1.
end

Algorithm 3 Pilot Sequence Claim

Data: Results of joint pilot and power control: $\mathbf{p}^*$

Result: Updated pilot assignment vector $\boldsymbol{\mu}$;

Initialization: Set $\mathcal{W}_g = \mathcal{W}, \forall g \in \mathcal{G}$;
  Set $\mu_{gw} = 1,\ \forall g \in \mathcal{G}, w \in \mathcal{W}$;
for *each user* $g \in \mathcal{G}$ **do**
  Set $\mu_{gw} = 0$ with $w^* = \arg\min_{w \in \mathcal{W}_g} p^*_{gw}$;
  Set $\mathcal{W}_g = \mathcal{W}_g \setminus w^*$;
end
if $\sum_{w \in \mathcal{W}} \mu_{gw} \leq 1$ *is satisfied for all users in* $\mathcal{G}$ **then**
  STOP;
else
  Run Algorithm 2;
  Go to Step 3.
end

Then, for each pilot sequence $w \in \mathcal{W}$, the effective SINR γ_g defined through (8)-(10) can be redefined as $\gamma_{gw}(\widetilde{\mathbf{p}})$ for each ground user $g \in \mathcal{G}$, as in (19) and (20), as shown at the bottom of the previous page. Then, Problem 2 in (16) can be reformulated as Problem 2 (reform):

$$\begin{aligned} &\textbf{Problem 2 (reform)} \\ &\text{Given}: \ \mathbf{x}^{(\nu)}, \mathbf{y}^{(\nu)}, \mathbf{z}^{(\nu)}, \boldsymbol{\alpha}^{(\nu+1)} \\ &\underset{\widetilde{\mathbf{p}}}{\text{Maximize}}: \ U \triangleq \sum_{g \in \mathcal{G}} \sum_{w \in \mathcal{W}} C_{gw}(\widetilde{\mathbf{p}}) \\ &\text{Subject to}: \ \mathit{Constraints}\ (17), (18), \end{aligned} \tag{21}$$

where $C_{gw}(\widetilde{\mathbf{p}}) = B \log_2(1 + \gamma_{gw}(\widetilde{\mathbf{p}}))$ with $\gamma_{gw}(\widetilde{\mathbf{p}})$ defined in (19) and (20). Next we solve Problem 2 (reform) in (21) by designing a distributed pricing-based solution algorithm.

Pricing-based Solution Algorithm. As illustrated in Fig. 2, the main idea of the pricing-based solution algorithm is to let each ground user iteratively determine its own pilot assignment and transmit power by maximizing a penalized version of its own utility in each iteration. Let $p_{gw}^{(\nu)}$ represent the power of ground user g when transmitting using pilot sequence w in current iteration ν. Define

$$\widetilde{\mathbf{p}}_g^{(\nu)} = (\log(p_{gw}^{(\nu)}))^{w \in \mathcal{W}}, \tag{22}$$

$$\widetilde{\mathbf{p}}_{-g}^{(\nu)} = (\log(p_{g'w}^{(\nu)}))_{g' \in \mathcal{G} \setminus g}^{w \in \mathcal{W}}. \tag{23}$$

Then the transmit power constraints in (17) and (18) can be rewritten as, in each iteration $\nu = 1, 2, \cdots$,

$$\widetilde{p}_{gw}^{(\nu)} \leq \log(p_{\max}), \quad \forall g \in \mathcal{G}, w \in \mathcal{W}\ , \tag{24}$$

$$\sum_{w \in \mathcal{W}} e^{\widetilde{p}_{gw}^{(\nu)}} \leq p_{\max}, \quad \forall g \in \mathcal{G}. \tag{25}$$

Then, the pricing-based solution algorithm can be formalized in Algorithm 2, where $U_g(\widetilde{\mathbf{p}}_g, \widetilde{\mathbf{p}}_{-g}^{(\nu)}) = \sum_{w \in \mathcal{W}} C_{gw}(\widetilde{\mathbf{p}}_g, \widetilde{\mathbf{p}}_{-g}^{(\nu)})$ is the individual rate achievable by ground user g, $\eta^{(\nu)}$ is the step size in iteration ν. The convergence of Algorithm 2 is given in Theorem 1.

Theorem 1: If Algorithm 2 *doesn't stop after certain number of iterations and suppose that the step-size sequence* $\{\eta^{(\nu)}\}$ *is chosen to satisfy*

$$\eta^{(\nu)} \in (0, 1], \eta^{(\nu)} \to 0, \sum_{\nu} \eta^{(\nu)} = +\infty, \tag{26}$$

then the algorithm converges to a stationary point of Problem 2 (reform) *defined in (27), as shown at the bottom of this page, and none of the stationary points is local minimum of the problem.*

Proof: We first show that the utility function of Problem 2 (reform) in (27) is a strongly concave function with respect to the transformed power control variables $\widetilde{\mathbf{p}}_g^{(\nu)}$ of ground user g with given control strategies $\widetilde{\mathbf{p}}_{-g}^{(\nu)}$ for the other users in $\mathcal{G} \setminus g$. Since the penalization item is an affine function of $\widetilde{\mathbf{p}}_g^{(\nu)}$ and the convexification item is strongly concave with $\psi_g > 0$, we only need to show that $U_g(\widetilde{\mathbf{p}}_g; \widetilde{\mathbf{p}}_{-g}^{(\nu)})$ is concave and the feasbile set defined by constraints (24) and (25) is convex. Consider high SINR in massive MIMO setting, i.e., $\gamma_{gw}(\widetilde{\mathbf{p}}) \gg 1$ in (19) and (20), then, with the logarithm transformation in (22) and (23), the achievable rate $R_{gw}(\widetilde{\mathbf{p}})$ in (21) can be represented in the form of *minus-log-sum-exp* and hence is a concave function [64]. Similarly, the left-hand side of constraint (25) has a form of *log-sum-exp* and hence

$$\begin{aligned} &\textbf{Problem 2 (penal)} \\ &\text{Given}: \quad \mathbf{x}, \mathbf{y}, \mathbf{z}, \boldsymbol{\alpha}, \ \widetilde{\mathbf{p}}^{(\nu)} \\ &\underset{\widetilde{\mathbf{p}}_g}{\text{Maximize}}: \quad U_g(\widetilde{\mathbf{p}}_g; \widetilde{\mathbf{p}}_{-g}^{(\nu)}) + \underbrace{\sum_{g' \in \mathcal{G} \setminus g} \nabla_{\widetilde{\mathbf{p}}_g} U_{g'}(\widetilde{\mathbf{p}}^{(\nu)})(\widetilde{\mathbf{p}}_g - \widetilde{\mathbf{p}}_g^{(\nu)})}_{Penalization\ Item} \underbrace{-\frac{\psi_g}{2}\|\widetilde{\mathbf{p}}_g - \widetilde{\mathbf{p}}_g^{(\nu)}\|^2}_{Convexification\ Item} \\ &\text{Subject to}: \quad \mathit{Constraints}\ (24), (25) \end{aligned} \tag{27}$$

the constraint defines a convex set. Then, the convergence of Algorithm 2 follows Theorem 3 in [65]. □

Remark 2: In Theorem 1, the conditions on the choice of step-size sequence $\{\eta^{(\nu)}\}$ is relatively weak; for instance all the step-size rules using in diminishing gradient-like schemes can be used here. The following are two effective rules [65], given $\eta^{(0)} = 1$:

$$\text{Rule 1}: \ \eta^{(\nu)} = \eta^{(\nu-1)}(1 - \epsilon\eta^{(\nu-1)}), \quad \nu = 1, 2, \cdots \tag{28}$$

$$\text{Rule 2}: \ \eta^{(\nu)} = \frac{\eta^{(\nu-1)} + \beta_1}{1 + \beta_2^{(\nu)}}, \quad \nu = 1, 2, \cdots \tag{29}$$

where $\epsilon \in (0, 1)$ and $\beta_1, \beta_2 \in (0, 1)$ are predefined constants with $\beta_1 < \beta_2$.

Pilot Sequence Claim. Recall in Section III that we consider that each ground user occupies at most one pilot sequence. This is accomplished by pilot sequence claim based on the results of the joint pilot and power allocation described above. Let $\mathbf{p}^* = (p^*_{gw})^{w\in\mathcal{W}}_{g\in\mathcal{G}}$ represent the output of Algorithm 2. Then the pilot sequence claim can be summarized in Algorithm 3 as follows, where the rationale of the pilot sequence claim is to let each user claim not to use the pilot sequence that has been allocated the least transmit power.

C. Movement Control

As illustrated in Fig. 2, in the third subproblem each drone determines its own best coordinates to adapt to the changes in association strategies and transmit power of the ground users resulting from solving the previous two subproblems. With the newly obtained association vector $\boldsymbol{\alpha}^{(\nu+1)}$ and transmit power vector $\mathbf{p}^{(\nu+1)}$, the subproblem of aerial drone movement can be written as, for each drone $a \in \mathcal{A}$,

$$\begin{aligned}
&\textbf{Problem 3}\\
&\text{Given}: \ \boldsymbol{\alpha}^{(\nu+1)}, \boldsymbol{\mu}^{(\nu+1)}, \mathbf{p}^{(\nu+1)}\\
&\underset{\mathbf{x},\,\mathbf{y},\,\mathbf{z}}{\text{Maximize}}: \ \sum_{g\in\mathcal{G}_a} C_g(\mathbf{x},\ \mathbf{y},\ \mathbf{z}),\\
&\text{Subject to}: \ x_{\min} \le x_a \le x_{\max}, \quad \forall a \in \mathcal{A},\\
&\qquad\qquad\ \ y_{\min} \le y_a \le y_{\max}, \quad \forall a \in \mathcal{A},\\
&\qquad\qquad\ \ z_{\min} \le z_a \le z_{\max}, \quad \forall a \in \mathcal{A},
\end{aligned} \tag{30}$$

where $\mathcal{G}_a$ represents the set of ground users associated with drone a with given access association vector $\boldsymbol{\alpha}^{(\nu+1)}$. In this subproblem, the mathematical expression of utility function $C_g(\mathbf{x},\ \mathbf{y},\ \mathbf{z})$ defined in (7) has a log-convex form, which is in general nonconcave with respect to coordinate variables $\mathbf{x}$, $\mathbf{y}$ and $\mathbf{z}$. In this paper we solve subproblem (30) using an interior point method [64] to search for locally-optimal coordinates for each aerial drone in favor of a low-complexity distributed solution.

D. Complexity Analysis

In the distributed solution algorithm, the above three subproblems are solved iteratively and sequentially at each iteration. In the ground-drone association subproblem, the association strategy is determined iteratively as well. In each iteration, the association variable α_{ga} can be determined for at least one ground node, and therefore the maximum number of associations is $|\mathcal{G}|$, and the overall computational complexity of the association is $\mathcal{O}(|\mathcal{G}|)$. The subproblem of joint power and pilot control in (27) and the aerial drone movement control subproblem (30) can be solved in polynomial computational complexity, i.e., $\mathcal{O}(|\mathcal{G}||\mathcal{A}|)$. Therefore, the complexity of the overall distributed solution algorithm is $\mathcal{O}(|\mathcal{G}|(|\mathcal{A}| + 1))$ for each iteration.

Summary: So far, we have presented a distributed solution algorithm for mDroneNet (i.e., wireless ad hoc networks with massive-MIMO drone hotspots) to jointly control the movement of the drone hotspots, the ground-drone association as well as power control and pilot sequence assignment for the ground users. A natural question is: *How does the distributed solution algorithm compare to the global optimum in terms of aggregate spectral efficiency?* In the remainder of the paper we answer this question by designing a centralized solution algorithm to provide a performance benchmark for the distributed solution algorithms.

V. Centralized Solution Algorithm

Recall from Section III that, in the social network control problem, i.e., Problem 1 in (11), the individual throughput $C_g(\boldsymbol{\alpha}, \boldsymbol{\mu}, \mathbf{p}, \mathbf{x}, \mathbf{y}, \mathbf{z})$ defined through (7)-(9) is a nonconvex/nonconcave function with respect to coordinates variables $\mathbf{x},\ \mathbf{y},\ \mathbf{z}$ and transmit power variables $\mathbf{p}$. Moreover, the association variables $\boldsymbol{\alpha}$ and pilot sequence assignment variables $\boldsymbol{\mu}$ take only binary values. Therefore the resulting network control problem is a mixed integer nonlinear nonconvex programming (MINLP) problem, for which there is in general no existing solution algorithm that can be used to obtain the global optimum in polynomial computational complexity. In this paper, we design a globally optimal solution algorithm based on *a combination of the branch and bound framework and of convex relaxation techniques* [66], [67]. Next we first describe the overall algorithm design framework.

A. Overall Algorithm

Denote $\boldsymbol{\Gamma}_0 = \{\boldsymbol{\alpha},\ \boldsymbol{\mu},\ \mathbf{p},\ \mathbf{x},\ \mathbf{y},\ \mathbf{z}|\ constraints\ in\ (11)\}$ as the feasible set of initial problem (11) and let $U^*(\boldsymbol{\Gamma}_0)$ represent the global optimum of problem (11) over $\boldsymbol{\Gamma}_0$, then the objective of our algorithm is to iteratively search for a U so that

$$U(\boldsymbol{\Gamma}_0) \ge \varepsilon U^*(\boldsymbol{\Gamma}_0), \tag{31}$$

where $\varepsilon \in (0, 1]$ is predefined optimality precision. To this end, the algorithm maintains a set $\boldsymbol{\Gamma} = \{\boldsymbol{\Gamma}_i,\ i = 0, 1, 2, \cdots\}$ of subproblems by iteratively partitioning feasible set $\boldsymbol{\Gamma}_0$ into a series of smaller subsets (see Section V-C).[6] The algorithm also maintains a global upper bound $\overline{U}_{\text{glb}}(\boldsymbol{\Gamma}_0)$ and a global lower bound $\underline{U}_{\text{glb}}(\boldsymbol{\Gamma}_0)$ on $U^*(\boldsymbol{\Gamma}_0)$ so that

$$\underline{U}_{\text{glb}}(\boldsymbol{\Gamma}_0) \le U^*(\boldsymbol{\Gamma}_0) \le \overline{U}_{\text{glb}}(\boldsymbol{\Gamma}_0) \tag{32}$$

to drive the iterations of subproblem partitions, as follows.

[6] In this paper we use $\boldsymbol{\Gamma}_i$ to refer to both subproblem i and the corresponding feasible set.

- *Global upper bound* $\overline{U}_{\rm glb}(\mathbf{\Gamma}_0)$: For each subproblem $\mathbf{\Gamma}_i \in \mathbf{\Gamma}$, the algorithm computes a local upper bound $\overline{U}_{\rm lcl}(\mathbf{\Gamma}_i)$ on network utility function U via *convex relaxation* (see Section V-B). Then the global upper bound $\overline{U}_{\rm glb}(\mathbf{\Gamma}_0)$ can be updated as

$$\overline{U}_{\rm glb}(\mathbf{\Gamma}_0) = \max_{\mathbf{\Gamma}_i \in \mathbf{\Gamma}} \{\overline{U}_{\rm lcl}(\mathbf{\Gamma}_i)\}. \tag{33}$$

- *Global lower bound* $\underline{U}_{\rm glb}(\mathbf{\Gamma}_0)$: Similarly, for each subproblem $\mathbf{\Gamma}_i \in \mathbf{\Gamma}$ a local lower bound $\underline{U}_{\rm lcl}(\mathbf{\Gamma}_i)$ is computed based on the solution obtained by solving the relaxed convex network control problem. Then the global lower bound $\underline{U}_{\rm glb}(\mathbf{\Gamma}_0)$ can be updated as

$$\underline{U}_{\rm glb}(\mathbf{\Gamma}_0) = \max_{\mathbf{\Gamma}_i \in \mathbf{\Gamma}} \{\overline{U}_{\rm lcl}(\mathbf{\Gamma}_i)\}. \tag{34}$$

The algorithm terminates if $\underline{U}_{\rm glb}(\mathbf{\Gamma}_0) \geq \varepsilon \overline{U}_{\rm glb}(\mathbf{\Gamma}_0)$ is reached and the global optimum $U^*(\mathbf{\Gamma}_0)$ is set to $U^*(\mathbf{\Gamma}_0) = \overline{U}_{\rm glb}(\mathbf{\Gamma}_0)$ as a upper-bound benchmark. Otherwise, the algorithm selects a subproblem from $\mathbf{\Gamma}$ and further partitions its feasible set into two smaller subsets, computes local upper and lower bounds and updates the global bounds $\overline{U}_{\rm glb}(\mathbf{\Gamma}_0)$ and $\underline{U}_{\rm glb}(\mathbf{\Gamma}_0)$ as in (33) and (34), respectively. In our algorithm, we select the subproblem $\mathbf{\Gamma}_i \in \mathbf{\Gamma}$ with the highest local upper bound to partition, i.e.,

$$\mathbf{\Gamma}_i = \arg\max_{\mathbf{\Gamma}_i} \overline{U}_{\rm lcl}(\mathbf{\Gamma}_i). \tag{35}$$

Based on the global bounds update criterion in (33) and (34), the gap between the two global bounds converges to 0 as the partition progresses. Furthermore, from (32), $\underline{U}_{\rm glb}(\mathbf{\Gamma}_0)$ and $\overline{U}_{\rm glb}(\mathbf{\Gamma}_0)$ converge to the global optimum $U^*(\mathbf{\Gamma}_0)$.

B. Convex Relaxation

For each subproblem $\mathbf{\Gamma}_i \subset \mathbf{\Gamma}$, which is MINLP in our case, a key step is to obtain a relaxed but convex version of $\mathbf{\Gamma}_i$ so that it is easy to compute a tight local upper bound $\overline{U}_{\rm lcl}(\mathbf{\Gamma}_i)$. In this paper the convex relaxation is designed following a two-phase approach as follows.

Phase 1: In this phase the relaxation is accomplished by assuming i) there is no mutual interference among ground nodes, i.e., interference items in the denominator of (8) are set to zero, and that all ground nodes use different pilot sequences in channel estimation and hence $\xi_{gg} = 0$ in (8); ii) the maximum number of the ground nodes that can be associated with a drone hotspot is not limited to $G_{\max}$ in (4). Then, the objective of the relaxed network control problem is to maximize the aggregate capacity of ground nodes by determining the optimal coordinate $\mathbf{x}$, $\mathbf{y}$ and $\mathbf{z}$ of the drones, i.e.,

Problem 4

$$\begin{aligned} \underset{\mathbf{x},\,\mathbf{y},\,\mathbf{z}}{\text{Maximize}}: \;& U \triangleq \sum_{g \in \mathcal{G}} C_g(\mathbf{x},\,\mathbf{y},\,\mathbf{z}) \\ \text{Subject to}: \;& x_{\min} \leq x_a \leq x_{\max}, \quad \forall a \in \mathcal{A}, \\ & y_{\min} \leq y_a \leq y_{\max}, \quad \forall a \in \mathcal{A}, \\ & z_{\min} \leq z_a \leq z_{\max}, \quad \forall a \in \mathcal{A}, \end{aligned} \tag{36}$$

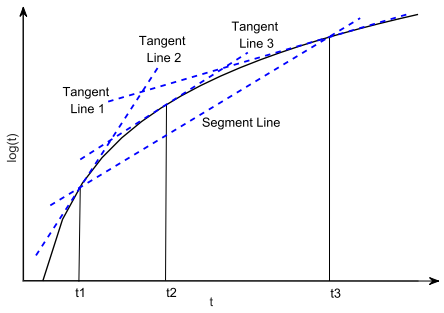

Fig. 3. Approximiation of log(t) using three tangent lines and one segment line.

where $C_g(\mathbf{x},\ \mathbf{y},\ \mathbf{z}) = B\log_2(1+\gamma_g(\mathbf{x},\ \mathbf{y},\ \mathbf{z}))$ with $\gamma_g(\mathbf{x},\ \mathbf{y},\ \mathbf{z})$ defined in (8). Since $\gamma_g(\mathbf{x},\ \mathbf{y},\ \mathbf{z}) \gg 1$, $R_g(\mathbf{x},\ \mathbf{y},\ \mathbf{z})$ can be approximated as

$$\begin{aligned} & C_g(\mathbf{x},\ \mathbf{y},\ \mathbf{z}) \\ & \approx B\log_2(\gamma_g(\mathbf{x},\ \mathbf{y},\ \mathbf{z})) && (37) \\ & \leq B\log_2\left(M\tau\rho_g p_0 \zeta_{gg}^2 H_{gg}^2(\mathbf{x},\ \mathbf{y},\ \mathbf{z})\right) && (38) \\ & = B\log_2\left(\frac{M\tau\rho_g p_0 \zeta_{gg}^2}{d_{gg}^{\chi}(\mathbf{x},\ \mathbf{y},\ \mathbf{z})}\right) && (39) \\ & = B\log_2(M\tau\rho_g p_0\zeta_{gg}^2) - \chi B\log_2(d_{gg}(\mathbf{x},\ \mathbf{y},\ \mathbf{z})), && (40) \end{aligned}$$

where the inequality in (38) holds since $G_{a(g)} \geq 0$ in (8), χ is path loss factor and $d_{gg}(\mathbf{x},\ \mathbf{y},\ \mathbf{z})$ is distance (in meter) from ground node g to its service aerial drone $a(g)$.

Since $d_{gg}(\mathbf{x},\ \mathbf{y},\ \mathbf{z})$ in (40) is a convex Euclidean norm with respect to $\mathbf{x}$, $\mathbf{y}$ and $\mathbf{z}$ [64], $\log_2(d_{gg}(\mathbf{x},\ \mathbf{y},\ \mathbf{z}))$ cannot be theoretically guaranteed to be concave. In this phase, we obtain a convex relaxation of (40) based on linear approximation of logarithmic function. To this end, we first replace $d_{gg}(\mathbf{x},\ \mathbf{y},\ \mathbf{z})$ in (40) with t, then $\log_2(d_{gg}(\mathbf{x},\ \mathbf{y},\ \mathbf{z})$ in (40) can be represented as $\log_2(t)$ subject to $t \geq d_{gg}(\mathbf{x},\ \mathbf{y},\ \mathbf{z})$. Then, $\log_2(t)$ can be further relaxed using a set of linear functions, e.g., as shown in Fig. 3, using a segment and three tangent lines.

Phase 2: Phase 2 of relaxation is invoked if the algorithm is done with partitioning coordinate variables $\mathbf{x}$, $\mathbf{y}$ and $\mathbf{z}$, i.e., for each aerial drone $a \in \mathcal{A}$,

$$x_{\max,a} - x_{\min,a} \leq \Delta x, \tag{41}$$

$$y_{\max,a} - y_{\min,a} \leq \Delta y, \tag{42}$$

$$z_{\max,a} - z_{\min,a} \leq \Delta z, \tag{43}$$

where $x_{\max,a}$ and $x_{\min,a}$ ($y_{\max,a}$ and $y_{\min,a}$) are upper and lower bounds of x-axis coordinate x_a (y-axis coordinate y_a), and Δx, Δy and Δz are predefined movement step size of aerial drones in x- and y-axis, respectively. The objective in this phase is to determine the optimal association vector $\boldsymbol{\alpha}$ with given aerial drones coordinates vectors $\mathbf{x}^*$, $\mathbf{y}^*$ and $\mathbf{z}^*$ and without considering mutual interference among ground nodes as in Phase 1 relaxation. Let C_{ga} represent the capacity achievable by ground node $g \in \mathcal{G}$ if g is associated to aerial drone $a \in \mathcal{A}$, then the optimal association can be obtained by

solving the following linear optimization problem:

Problem 5

$$\begin{aligned}
&\text{Given}: \ \mathbf{x}^*,\ \mathbf{y}^*,\ \mathbf{z}^*\\
&\underset{\boldsymbol{\alpha}}{\text{Maximize}}: \ \sum_{a\in\mathcal{A}}\sum_{g\in\mathcal{G}}\alpha_{ga}C_{ga}(\boldsymbol{\alpha},\ \mathbf{x}^*,\mathbf{y}^*,\ \mathbf{z}^*)\\
&\text{Subject to}: \ 0\le\alpha_{ga}\le 1, \quad \forall a\in\mathcal{A},\ g\in\mathcal{G},\\
&\qquad\qquad \sum_{g\in\mathcal{G}}\alpha_{ga}\le G_{\max}, \quad \forall a\in\mathcal{A},\\
&\qquad\qquad \sum_{a\in\mathcal{A}}\alpha_{ga}\le 1, \quad \forall g\in\mathcal{G}. \qquad (44)
\end{aligned}$$

As variable partition progresses, the association variable α_{ga} becomes fixed either to 0 or 1 in all subproblems, for which the optimal transmit power $\mathbf{p}$ and pilot sequence assignment $\boldsymbol{\mu}$ can be obtained by solving a geometric programming problem as in Section IV.

C. Variable Partition

Variable partition can be conducted by partitioning association variable $\boldsymbol{\alpha}$ and movement variables $\mathbf{x}$, $\mathbf{y}$ and $\mathbf{z}$. For example, given a subproblem $\boldsymbol{\Gamma}_i \in \boldsymbol{\Gamma}$, by fixing association variable α_{ga} subproblem $\boldsymbol{\Gamma}_i$ can be partitioned into two subproblems with feasible sets $\boldsymbol{\Gamma}_{i,1} = \{(\boldsymbol{\alpha},\ \mathbf{p},\ \mathbf{x},\ \mathbf{y},\ \mathbf{z}) \in \boldsymbol{\Gamma}_i | \alpha_{ga} = 0\}$ and $\boldsymbol{\Gamma}_{i,2} = \{(\boldsymbol{\alpha},\ \mathbf{p},\ \mathbf{x},\ \mathbf{y},\ \mathbf{z}) \in \boldsymbol{\Gamma}_i | \alpha_{ga} = 1\}$, respectively. For movement variables, say $x_a \in [x_{\min,a}\ \ x_{\max,a}]$ for aerial drone $a \in \mathcal{A}$, the partition can be conducted by splitting x_a from the half, resulting in two subproblems with feasible sets

$$\boldsymbol{\Gamma}_{i,1} = \{(\boldsymbol{\alpha},\mathbf{p},\mathbf{x},\mathbf{y},\mathbf{z}) \in \boldsymbol{\Gamma}_i | x_a \in [x_{\min,a}\ \ x_{\mathrm{mid},a}]\}, \quad (45)$$

$$\boldsymbol{\Gamma}_{i,2} = \{(\boldsymbol{\alpha},\mathbf{p},\mathbf{x},\mathbf{y},\mathbf{z}) \in \boldsymbol{\Gamma}_i | x_a \in [x_{\mathrm{mid},a}\ \ x_{\max,a}]\}, \quad (46)$$

where $x_{\mathrm{mid},a} \triangleq \frac{x_{\min,a}+x_{\max,a}}{2}$. As variable partition progresses, the algorithm converges to the global optimum, as stated in the following theorem.

Theorem 2: With convex relaxation the variable partition strategies in Sections V-B and V-C, global upper bound $\overline{U}_{\mathrm{glb}}$ and global lower bound $\underline{U}_{\mathrm{glb}}$ converge to the global optimum U^* of the original social network control problem formulated in (11).

Proof: To show convergence of the globally optimal solution algorithm, it is sufficient to show that the algorithm converges with respect to aerial drone movement variables $\mathbf{x}$, $\mathbf{y}$ and $\mathbf{z}$ since i) there is a finite number of possible combinations of association strategies for a given set $\mathcal{A}$ of aerial drones and set $\mathcal{G}$ of ground nodes, and ii) the power control subproblem is a convex optimization problem.

For this purpose, we first redefine the domain set based on the notation of hyper-rectangle. The initial ranges of aerial drone movement variables x_a, y_a and z_a for each aerial drone $a \in \mathcal{A}$ are $[0\ \ x_{\max}]$, $[0\ \ y_{\max}]$ and $[0\ \ z_{\max}]$, respectively. This results in an initial feasible set, which is an $L = 2|\mathcal{A}|$-dimensional hyper-rectangle denoted as $\boldsymbol{\Gamma}_{\mathrm{init}}$ with $|\mathcal{A}|$ being the number of aerial drones in $\mathcal{A}$. As in Section V, denote $\boldsymbol{\Gamma}$ as the set of sub-rectangles obtained from partitioning $\boldsymbol{\Gamma}_{\mathrm{init}}$ as the iteration goes. For any sub-rectangle $\widetilde{\boldsymbol{\Gamma}} \in \boldsymbol{\Gamma}$, denote v^l_{upp} and v^l_{lwr} as the upper and lower bound of the l^{th} edge of the rectangle with $l = 1, \cdots, L$. For example, for the x-axis of the initial domain set $\boldsymbol{\Gamma}_{\mathrm{init}}$, we have $v^l_{\mathrm{lwr}} = 0$ and $v^l_{\mathrm{upp}} = x_{\max}$. Further define the size, volume (vol), and condition number (cond) of $\widetilde{\boldsymbol{\Gamma}}$ as follows:

- $\mathrm{size}(\widetilde{\boldsymbol{\Gamma}}) \equiv \max\limits_{l=1,\cdots,L} \frac{1}{2}(v^l_{\mathrm{upp}} - v^l_{\mathrm{lwr}})$, i.e., the maximum of half edge length;
- $\mathrm{vol}(\widetilde{\boldsymbol{\Gamma}}) \equiv \prod\limits_{l=1,\cdots,L} (v^l_{\mathrm{upp}} - v^l_{\mathrm{lwr}})$, i.e., the edge length production;
- $\mathrm{cond}(\widetilde{\boldsymbol{\Gamma}}) \equiv \frac{\max\limits_{l=1,\cdots,L}(v^l_{\mathrm{upp}} - v^l_{\mathrm{lwr}})}{\min\limits_{l=1,\cdots,L}(P^l_{\mathrm{upp}} - P^l_{\mathrm{lwr}})}$, i.e., the ratio of the maximum and the minimum edge lengths.

Then, considering the domain partition strategy described in Section V (i.e., in each iteration, partition the variable that has the largest range from its middle), after a sufficiently large number of iterations, say k, the following inequality holds:

$$\min_{\widetilde{\Gamma}\in\Gamma} \mathrm{size}(\widetilde{\boldsymbol{\Gamma}}) \le \max\{\mathrm{cond}(\Gamma_{\mathrm{init}}), 2\}\left(\frac{\mathrm{vol}(\Gamma_{\mathrm{init}})}{k}\right), \quad (47)$$

which implies that the minimum size (hence the largest range of movement variables) in all subproblems converges to zero as $k \to \infty$, i.e., the ranges of aerial drone movement variables x_a and y_a shrink to constant for all drones $a \in \mathcal{A}$.

Denote $\widetilde{\boldsymbol{\Gamma}}^*$ as the sub-rectangle with the smallest size. Then, inequality (47) further implies that the local upper and lower bounds over $\widetilde{\boldsymbol{\Gamma}}^*$, i.e., $\underline{U}(\widetilde{\boldsymbol{\Gamma}}^*)$ and $\overline{U}(\widetilde{\boldsymbol{\Gamma}}^*)$, converge to each other if i) it holds for any sub-rectangle $\widetilde{\boldsymbol{\Gamma}} \in \Gamma$ that the local upper bound $\overline{U}(\widetilde{\boldsymbol{\Gamma}})$ is non-increasing as $\widetilde{\boldsymbol{\Gamma}}$ shrinks, which is true because that the algorithm partitions aerial drone movement variables ($\mathbf{x}$, $\mathbf{y}$ and $\mathbf{z}$) from their middle, and ii) the local upper bounds $\underline{U}(\widetilde{\boldsymbol{\Gamma}})$) are non-increasing, which follows that the highest local lower bound is always used in the algorithm.

Then, as the local upper and lower bounds over $\widetilde{\boldsymbol{\Gamma}}^*$ converge to each other, we can find a $\delta > 0$ for any optimality precision $\epsilon \in (0\ \ 1)$ such that any sub-rectangle $\widetilde{\boldsymbol{\Gamma}}$ with $\mathrm{size}(\widetilde{\boldsymbol{\Gamma}}) \le \delta$ satisfies $\underline{U}(\widetilde{\boldsymbol{\Gamma}}) \ge \varepsilon\overline{U}(\widetilde{\boldsymbol{\Gamma}})$. Take the iteration index k sufficiently large so that the size of all sub-rectangles in $\widetilde{\boldsymbol{\Gamma}}$ do not exceed δ, then we have $\underline{U}_{\mathrm{glb}} = \max\limits_{\widetilde{\boldsymbol{\Gamma}}\in\boldsymbol{\Gamma}} \underline{U}(\widetilde{\boldsymbol{\Gamma}}) \ge \varepsilon \max\limits_{\widetilde{\boldsymbol{\Gamma}}\in\boldsymbol{\Gamma}} \overline{U}(\widetilde{\boldsymbol{\Gamma}}) = \overline{U}_{\mathrm{glb}}$. □

VI. Performance Evaluation

We evaluate the performance of the proposed network control solution algorithms by considering a network area of $500 \times 500\ \mathrm{m}^2$ while the altitude of the drone hotspots is set to 100 meters for simplicity of the simulations. The number of the ground users is set to $\{2, 4, 6, 8, 10, 12\}$, and the number of the drone hotspots is set to $\{2, 3\}$. The number of antennas of each drone hotspot is set to $\{10, 20, 30, 40, 50, 100\}$. The maximum transmit power of each ground user is set to $\{20, 40, 60, \cdots, 500\}$ mW. The path loss factor is set to $\chi = 2$, and the average noise power is set to 10^{-8} mW. The number of the available pilot sequences is set to $\{6, 8\}$, and the length of each pilot sequence is set to 10 symbols. The results are obtained by averaging over 20 independent simulation instances with network topology randomly generated. Next, we first discuss the convergence of the distributed and centralized solution algorithms, and then evaluate the optimality

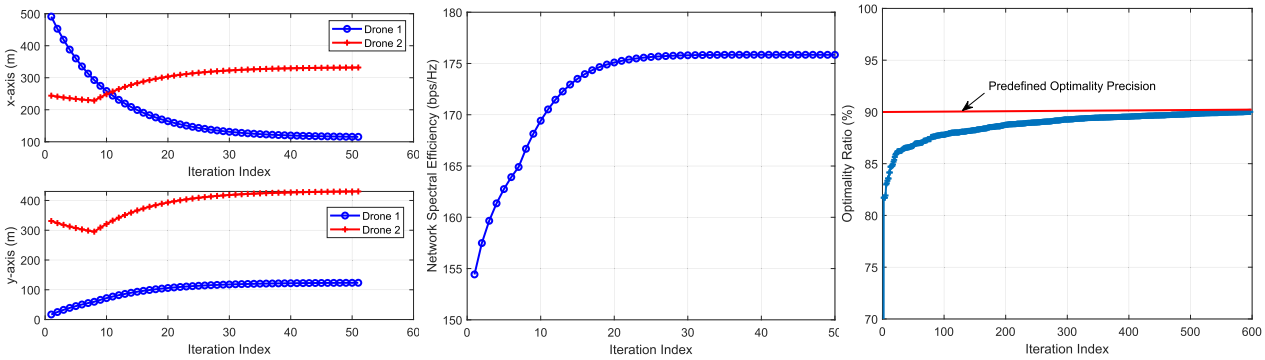

Fig. 4. (a) x- and y-axis of the drone hotspots and (b) aggregate network spectral efficiency with the distributed solution algorithm; (c) optimality ratio with the centralized solution algorithm.

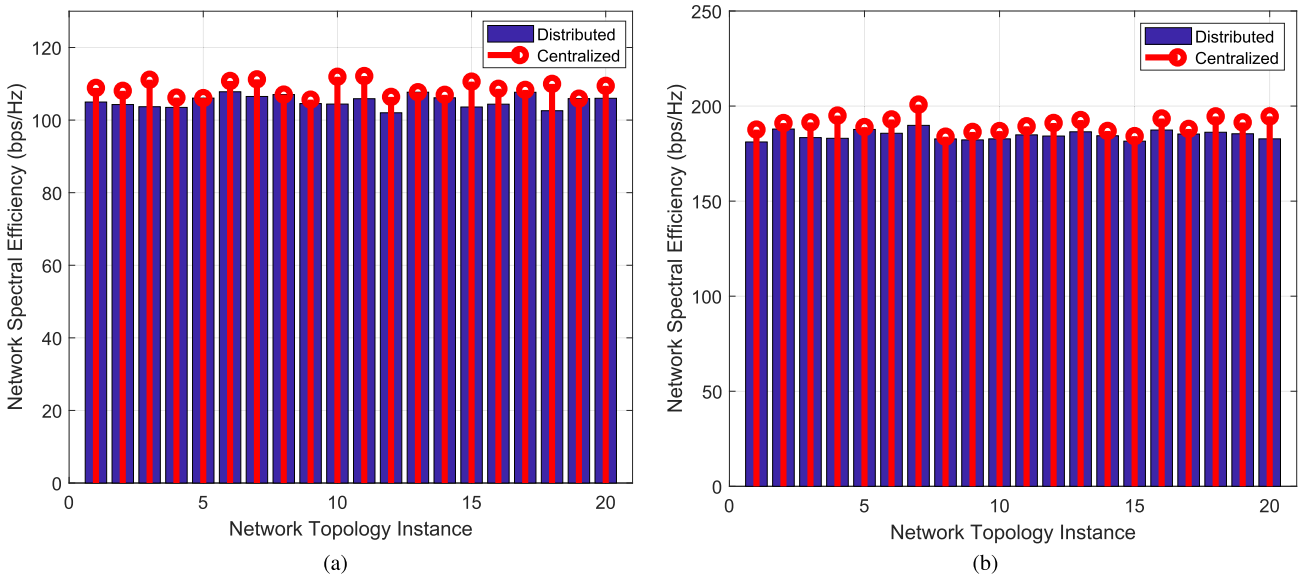

Fig. 5. Aggregate network spectral efficiency with the distributed and centralized solution algorithms with (a) 4 ground users, 2 drone hotspots with each having 100 antennas, and 8 pilot sequences, and (b) 8 ground users, 2 drone hotspots with each having 20 antennas, and 6 pilot sequences.

of the distributed solution algorithm by comparing it to the centralized. Finally we study the effects of different network control strategies on the aggregate network spectral efficiency.

Convergence. The convergence of the distributed solution algorithm and the centralized solution algorithm is shown in Fig. 4. In Fig. 4(a), two drone hotspots and eight ground users are considered and the initial locations of the drones are randomly generated within the networking area. It can be seen that the movement of the drone hotspots converge quickly in around 40 iterations. In Fig. 4(b) we plot the resulting aggregate network spectral efficiency of all the ground users. It can be seen that the network spectral efficiency converges quickly as well. The convergence of the centralized solution algorithm is shown in Fig. 4(c). The optimality precision is set to 90% and the maximum number of iterations is set to 5000. In can be seen that the optimality ratio converges monotonically as the interation progresses and the predefined optimality precision is reached in 600 iterations. The computational complexity of the distributed and centralized solution algorithms is compared in terms of the number of iterations required to converge in the case of different number of ground nodes. We tested 20 more network instances with the number of ground nodes varying from 2 to 10. Results showed that both the distributed and centralized solution algorithms converge in all the tested instances. With distributed solution algorithms it takes on average 25 iterations to coverage, e.g., 15, 26 and 35 iterations in the cases of 2, 8 and 10 ground nodes, respectively. The centralized solution algorithm takes more iterations than the distributed to converge. For example, it takes 4592 iterations for the centralized solution algorithm to converge in the case of 8 ground nodes and 4688 iterations on average. It is worth pointing out that while the centralized solution algorithm has higher computational complexity, the objective of the centralized solution algorithm is to provide a benchmark performance for the distributed solution algorithm.

Optimality. Figure 5 reports the network spectral efficiency, i.e., the spectral efficiency summed over all the users in the network, achievable by the distributed solution algorithm and the centralized global optimum. Four ground users, 2 drone hotspots and 8 pilot sequences are considered

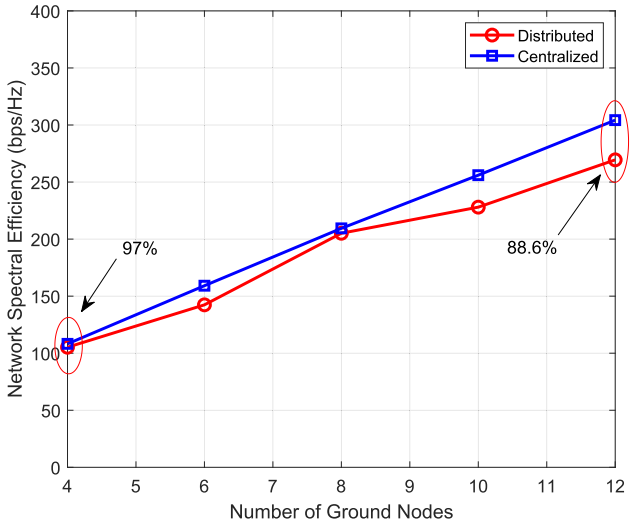

Fig. 6. Network spectral efficiency in the case of different number of ground users.

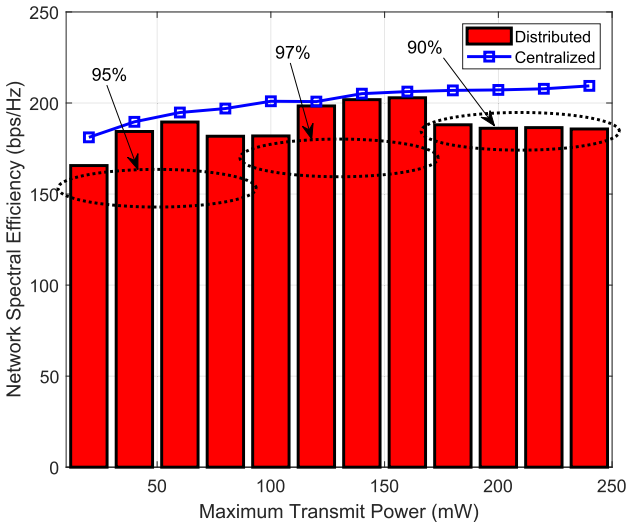

Fig. 7. Network spectral efficiency in the case of different maximum transmit power for the ground users.

in Fig. 5(a) while 8 ground users, 2 drones and 6 pilot sequences in Fig. 5(b). It can be seen that in both cases the distributed solution algorithm achieves an aggregate network spectral efficiency very close to the global optimum in all of the 20 tested network topology instances, with average optimality of 97% and 91% for Figs. 5(a) and (b), respectively. Comparing Fig. 5(b) to Fig. 5(a) it can be found that, as expected, the aggregate network spectral efficiency increases as more users are accommodated in the network, e.g., from 105 bps/Hz to 165 bps/Hz for the distributed solution algorithm.

The average performance of the achievable network spectral efficiency is reported in Fig. 6 with different number of ground users. Results indicate that in average around 92.5% of the global optimum can be achieved by the distributed solution algorithm, and the optimality is 97%, 98% and 88.6% with 4, 8 and 12 ground users, respectively. It is also noticed that the achievable network spectral efficiency increases linearly with the number of the served ground users in the setting of the considered mDroneNet.

In Fig. 7 we plotted the achievable network spectral efficiency against the maximum transmit power of the ground users. Eight ground users and 2 drone hotspots each having 100 antennas are considered in this experiment. On average over 93% of the global optimum can be achieved by the distributed solution algorithms, with 95%, 97% and 90% for transmit power in [20 80] mW, [100 160] mW and [180 220] mW, respectively. From the results of the centralized solution algorithm we noticed that the aggregate network spectral efficiency rises only around 4.5% by increasing the maximum transmit power by 2.4 times from 100 to 240 mW. This is because in massive MIMO setting the network basically operates at high SINR regime, i.e., in bandwidth-limited regime.

The network spectral efficiency is reported in Fig. 8 with the number of antennas for each drone hotspot varies from 20 to 100, with 8 ground users and 6 pilot sequences. The distributed network control strategy achieves on average over

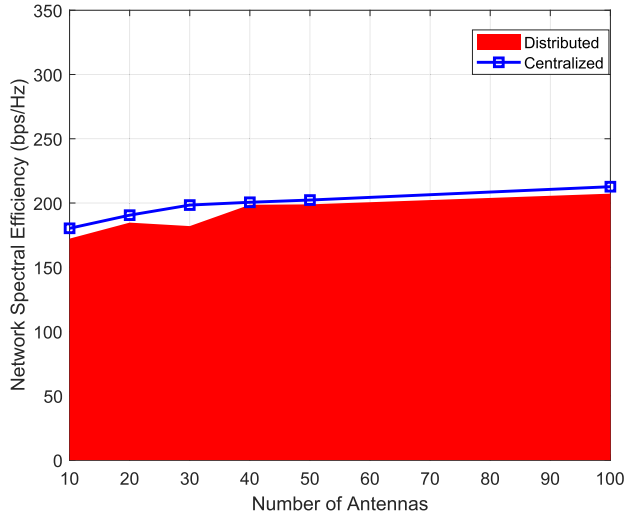

Fig. 8. Network spectral efficiency in the case of different number of antennas for the drone hotspots.

93.5% of the global optimum obtained by the centralized solution algorithm. We notice that the achievable network spectral efficiency monotonically increases with the number of antennas but at a decreasing speed. This is consistent with the results in [9, Fig. 4(a)]. It is worth pointing out that, comparing to [9, Fig. 4(a)], the network spectral efficiency gain achievable by using more antennas is less significant in our case, e.g., in this experiment the effect of increasing the number of antennas is only marginal if each drone hotspot has more than 30 antennas. This is because our objective is to study joint power, association and flight control in self-organizing massive-MIMO-enabled UAV networks, and in this setting the network spectral efficiency is jointly determined by all the affecting factors. As a future research direction we will study how many antennas are required to achieve certain spectral efficiency in self-organizing UAV networks.

We further study the effects of different network control strategies on the achievable network spectral efficiency

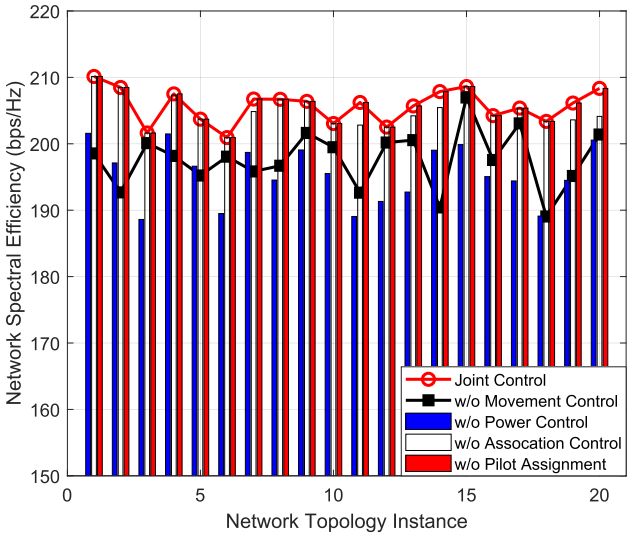

Fig. 9. Network spectral efficiency achievable with different network control strategies: 12 ground users, 2 drone hotspots.

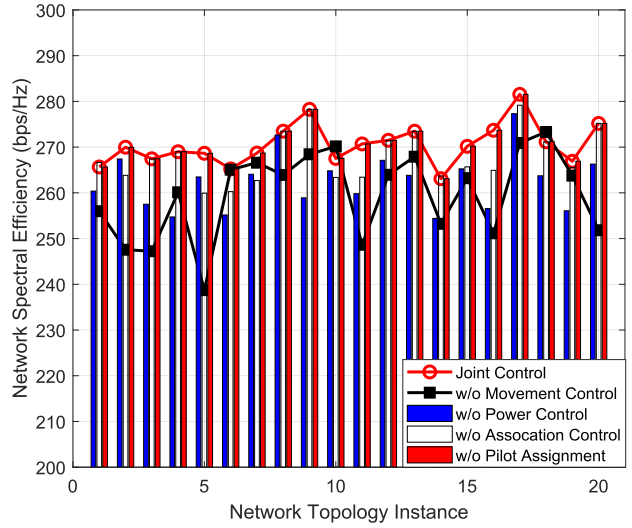

Fig. 10. Network spectral efficiency achievable with different network control strategies: 12 ground users, 3 drone hotspots.

through Figs. 9-10, where the joint network control strategy is compared to the other four strategies: (i) the locations of the drone hotspots are randomly generated in "w/o Aerial Drone Movement"; (ii) the transmit power is randomly generated for the ground users in "w/o Power Control"; (iii) the access association is executed only once in "w/o Association Control"; and (iv) the pilot sequence assignment is executed only once in "w/o Pilot Assignment". In Fig. 9 the experiment considers 12 ground users sharing 6 pilot sequences and 2 drone hotspots each having 100 antennas. We can see that the joint network control achieves the highest aggregate network spectral efficiency in almost all of the tested instances. An obvious performance degradation can be observed without power control for the ground users or movement control for the drone hotspots, which are 5% and 4% on average, respectively. It can also be noticed that a spectral efficiency very close to that of joint control can be achieved by "w/o Association Control" and "w/o Pilot Assignment". This implies that only one-time access association and one-time pilot assignment would be sufficient in the joint network control. Similar results are reported in Fig. 10 where three drone hotspots are used to serve 12 ground users with each drone endowed with 100 antennas. Unsurprisingly, the aggregate network spectral efficiency can be significantly improved by using more drone hotspots, while the performance degradation because of the lack of power control reduces to less than 4% on average.

VII. Conclusions

We studied wireless ad hoc networking with massive-MIMO drone hotspots. The network control objective is to maximize network-wide spectral efficiency by jointly controlling the movement of the drones, associating single-antenna ground nodes to many-antenna drones, and adapting the transmit power as well as the pilot sequence assignment for the ground nodes. The network control problem was formulated as a mixed integer nonlinear nonconvex programming (MINLP) problem. Both distributed and globally optimal solution algorithms have been designed and evaluated with extensive simulation results. Results indicated that the distributed solution algorithm converges within tens of iterations and can achieve around 90% of the global optimum.

Acknowledgment

Any opinions, findings and conclusions or recommendations expressed in this material are those of the author(s) and do not necessarily reflect the views of AFRL.

References

[1] Z. Guan, N. Cen, T. Melodia, and S. Pudlewski, "Self-organizing flying drones with massive MIMO networking," in *Proc. 17th Annu. Medit. Ad Hoc Netw. Workshop (Med-Hoc-Net)*, Capri, Italy, Jun. 2018, pp. 1–8.

[2] Y. Liu and S. Das, "Information-intensive wireless sensor networks: Potential and challenges," *IEEE Commun. Mag.*, vol. 44, no. 11, pp. 142–147, Nov. 2006.

[3] V. J. Hodge, S. O'Keefe, M. Weeks, and A. Moulds, "Wireless sensor networks for condition monitoring in the railway industry: A survey," *IEEE Trans. Intell. Transp. Syst.*, vol. 16, no. 3, pp. 1088–1106, Jun. 2015.

[4] R. Iyer, "Visual IoT: Architectural challenges and opportunities," *IEEE Micro*, vol. 36, no. 6, pp. 45–49, Nov./Dec. 2016.

[5] J. Gubbi, R. Buyya, S. Marusic, and M. Palaniswami, "Internet of Things (IoT): A vision, architectural elements, and future directions," *Future Gener. Comput. Syst.*, vol. 29, no. 7, pp. 1645–1660, Sep. 2013.

[6] M. Deruyck, J. Wyckmans, L. Martens, and W. Joseph, "Emergency ad-hoc networks by using drone mounted base stations for a disaster scenario," in *Proc. IEEE 12th Int. Conf. Wireless Mobile Comput., Netw. Commun. (WiMob)*, Oct. 2016, pp. 1–7.

[7] M. Noura and R. Nordin, "A survey on interference management for Device-to-Device (D2D) communication and its challenges in 5G networks," *J. Netw. Comput. Appl.*, vol. 71, pp. 130–150, Aug. 2016.

[8] S. Ali and A. Ahmad, "Resource allocation, interference management, and mode selection in device-to-device communication: A survey," *Trans. Emerg. Telecommun. Technol.*, vol. 28, no. 7, p. e3148, Jul. 2017.

[9] E. Björnson, E. G. Larsson, and T. L. Marzetta, "Massive MIMO: Ten myths and one critical question," *IEEE Commun. Mag.*, vol. 54, no. 2, pp. 114–123, Feb. 2016.

[10] M. Mozaffari, W. Saad, M. Bennis, Y.-H. Nam, and M. Debbah, "A tutorial on UAVs for wireless networks: Applications, challenges, and open problems," *IEEE Commun. Surveys Tuts.*, vol. 21, no. 3, pp. 2334–2360, 3rd Quart., 2019.

[11] K. A. Swieringa *et al.*, "Autonomous battery swapping system for small-scale helicopters," in *Proc. IEEE Int. Conf. Robot. Autom.*, Anchorage, AK, USA, May 2010, pp. 3335–3340.

[12] B. Michini *et al.*, "Automated battery swap and recharge to enable persistent UAV missions," in *Proc. Infotech@Aerospace*, Mar. 2011, pp. 1–10.

[13] A. Trotta, M. Di Felice, K. R. Chowdhury, and L. Bononi, "Fly and recharge: Achieving persistent coverage using small unmanned aerial vehicles (SUAVs)," in *Proc. IEEE Int. Conf. Commun. (ICC)*, Paris, France, May 2017, pp. 1–7.

[14] M. Shin, J. Kim, and M. Levorato, "Auction-based charging scheduling with deep learning framework for multi-drone networks," *IEEE Trans. Veh. Technol.*, vol. 68, no. 5, pp. 4235–4248, May 2019.

[15] H. Quoc Ngo, E. G. Larsson, and T. L. Marzetta, "Energy and spectral efficiency of very large multiuser MIMO systems," *IEEE Trans. Commun.*, vol. 61, no. 4, pp. 1436–1449, Apr. 2013.

[16] T. L. Marzetta, "Noncooperative cellular wireless with unlimited numbers of base station antennas," *IEEE Trans. Wireless Commun.*, vol. 9, no. 11, pp. 3590–3600, Nov. 2010.

[17] J. Zhu, R. Schober, and V. K. Bhargava, "Secure transmission in multicell massive MIMO systems," *IEEE Trans. Wireless Commun.*, vol. 13, no. 9, pp. 4766–4781, Sep. 2014.

[18] Y. Wu, R. Schober, D. W. K. Ng, C. Xiao, and G. Caire, "Secure massive MIMO transmission with an active eavesdropper," *IEEE Trans. Inf. Theory*, vol. 62, no. 7, pp. 3880–3900, Jul. 2016.

[19] E. G. Larsson, O. Edfors, F. Tufvesson, and T. L. Marzetta, "Massive MIMO for next generation wireless systems," *IEEE Commun. Mag.*, vol. 52, no. 2, pp. 186–195, Feb. 2014.

[20] T. L. Marzetta, "Massive MIMO: An introduction," *Bell Labs Tech. J.*, vol. 20, pp. 12–22, Mar. 2015.

[21] E. Bjornson, J. Hoydis, and L. Sanguinetti, "Massive MIMO has unlimited capacity," *IEEE Trans. Wireless Commun.*, vol. 17, no. 1, pp. 574–590, Jan. 2018.

[22] A. Garcia-Rodriguez, G. Geraci, L. G. Giordano, A. Bonfante, M. Ding, and D. Lopez-Perez, "Massive MIMO unlicensed: A new approach to dynamic spectrum access," *IEEE Commun. Mag.*, vol. 56, no. 6, pp. 186–192, Jun. 2018.

[23] D. Bethanabhotla, O. Y. Bursalioglu, H. C. Papadopoulos, and G. Caire, "Optimal user-cell association for massive MIMO wireless networks," *IEEE Trans. Wireless Commun.*, vol. 15, no. 3, pp. 1835–1850, Mar. 2016.

[24] J. Zhu and W. Xu, "Securing massive MIMO via power scaling," *IEEE Commun. Lett.*, vol. 20, no. 5, pp. 1014–1017, May 2016.

[25] K. Zheng, L. Zhao, J. Mei, B. Shao, W. Xiang, and L. Hanzo, "Survey of large-scale MIMO systems," *IEEE Commun. Surveys Tuts.*, vol. 17, no. 3, pp. 1738–1760, 3rd Quart., 2015.

[26] H. A. Suraweera, H. Q. Ngo, T. Q. Duong, C. Yuen, and E. G. Larsson, "Multi-pair amplify-and-forward relaying with very large antenna arrays," in *Proc. IEEE Int. Conf. Commun. (ICC)*, Budapest, Hungary, Jun. 2013, pp. 4635–4640.

[27] S. Jin, X. Liang, K.-K. Wong, X. Gao, and Q. Zhu, "Ergodic rate analysis for multipair massive MIMO two-way relay networks," *IEEE Trans. Wireless Commun.*, vol. 14, no. 3, pp. 1480–1491, Mar. 2015.

[28] G. Amarasuriya, "Sum rate analysis for multi-user massive MIMO relay networks," in *Proc. IEEE Global Commun. Conf. (GLOBECOM)*, San Diego, CA, USA, Dec. 2015, pp. 1–7.

[29] H. Q. Ngo, H. A. Suraweera, M. Matthaiou, and E. G. Larsson, "Multipair full-duplex relaying with massive arrays and linear processing," *IEEE J. Sel. Areas Commun.*, vol. 32, no. 9, pp. 1721–1737, Sep. 2014.

[30] Z. Zhang, Z. Chen, M. Shen, and B. Xia, "Spectral and energy efficiency of multipair two-way full-duplex relay systems with massive MIMO," *IEEE J. Sel. Areas Commun.*, vol. 34, no. 4, pp. 848–863, Apr. 2016.

[31] L. Lu, G. Y. Li, A. L. Swindlehurst, A. Ashikhmin, and R. Zhang, "An overview of massive MIMO: Benefits and challenges," *IEEE J. Sel. Topics Signal Process.*, vol. 8, no. 5, pp. 742–758, Oct. 2014.

[32] D. C. Araújo, T. Maksymyuk, A. L. F. de Almeida, T. Maciel, J. C. M. Mota, and M. Jo, "Massive MIMO: Survey and future research topics," *IET Commun.*, vol. 10, no. 15, pp. 1938–1946, Oct. 2016.

[33] V. Sharma and R. Kumar, "A cooperative network framework for multi-UAV guided ground ad hoc networks," *J. Intell. Robotic Syst.*, vol. 77, nos. 3–4, pp. 629–652, Mar. 2015.

[34] I. Jawhar, N. Mohamed, J. Al-Jaroodi, and S. Zhang, "A framework for using unmanned aerial vehicles for data collection in linear wireless sensor networks," *J. Intell. Robotic Syst.*, vol. 74, nos. 1–2, pp. 437–453, Apr. 2014.

[35] F. Ono, H. Ochiai, and R. Miura, "A wireless relay network based on unmanned aircraft system with rate optimization," *IEEE Trans. Wireless Commun.*, vol. 15, no. 11, pp. 7699–7708, Nov. 2016.

[36] L. Sboui, H. Ghazzai, Z. Rezki, and M.-S. Alouini, "Achievable rates of UAV-relayed cooperative cognitive radio MIMO systems," *IEEE Access*, vol. 5, pp. 5190–5204, 2017.

[37] S. Kandeepan, K. Gomez, L. Reynaud, and T. Rasheed, "Aerial-terrestrial communications: Terrestrial cooperation and energy-efficient transmissions to aerial base stations," *IEEE Trans. Aerosp. Electron. Syst.*, vol. 50, no. 4, pp. 2715–2735, Oct. 2014.

[38] K. Daniel, S. Rohde, N. Goddemeier, and C. Wietfeld, "Cognitive agent mobility for aerial sensor networks," *IEEE Sensors J.*, vol. 11, no. 11, pp. 2671–2682, Nov. 2011.

[39] D. H. Choi, S. H. Kim, and D. K. Sung, "Energy-efficient maneuvering and communication of a single UAV-based relay," *IEEE Trans. Aerosp. Electron. Syst.*, vol. 50, no. 3, pp. 2320–2327, Jul. 2014.

[40] T. J. Willink, C. C. Squires, G. W. K. Colman, and M. T. Muccio, "Measurement and characterization of low-altitude air-to-ground MIMO channels," *IEEE Trans. Veh. Technol.*, vol. 65, no. 4, pp. 2637–2648, Apr. 2016.

[41] P. Ladosz, H. Oh, and W.-H. Chen, "Optimal positioning of communication relay unmanned aerial vehicles in urban environments," in *Proc. Int. Conf. Unmanned Aircr. Syst. (ICUAS)*, Arlington, VA USA, Jun. 2016, pp. 1140–1147.

[42] Y. Zhou, M. Chen, and C. Jiang, "Robust tracking control of uncertain MIMO nonlinear systems with application to UAVs," *IEEE/CAA J. Automatica Sinica*, vol. 2, no. 1, pp. 25–32, Jan. 2015.

[43] D. Orfanus, E. P. de Freitas, and F. Eliassen, "Self-organization as a supporting paradigm for military UAV relay networks," *IEEE Commun. Lett.*, vol. 20, no. 4, pp. 804–807, Apr. 2016.

[44] S. Morgenthaler, T. Braun, Z. Zhao, T. Staub, and M. Anwander, "UAVNet: A mobile wireless mesh network using unmanned aerial vehicles," in *Proc. IEEE Globecom Workshops*, Dec. 2012, pp. 1603–1608.

[45] M. A. M. Marinho, E. P. de Freitas, J. P. C. Lustosa da Costa, A. L. F. de Almeida, and R. T. de Sousa, "Using cooperative MIMO techniques and UAV relay networks to support connectivity in sparse wireless sensor networks," in *Proc. Int. Conf. Comput., Manage. Telecommun. (ComManTel)*, Jan. 2013, pp. 49–54.

[46] P. Zhan, K. Yu, and A. L. Swindlehurst, "Wireless relay communications with unmanned aerial vehicles: Performance and optimization," *IEEE Trans. Aerosp. Electron. Syst.*, vol. 47, no. 3, pp. 2068–2085, Jul. 2011.

[47] I. Bekmezci, O. K. Sahingoz, and Ş. Temel, "Flying ad-hoc networks (FANETs): A survey," *Ad Hoc Netw.*, vol. 11, no. 3, pp. 1254–1270, May 2013.

[48] G. Chmaj and H. Selvaraj, "Distributed processing applications for UAV/drones: A survey," in *Proc. Int. Conf. Syst. Eng., Adv. Intell. Syst. Comput.*, Las Vegas, NV, USA, Aug. 2015, pp. 449–454.

[49] L. Gupta, R. Jain, and G. Vaszkun, "Survey of important issues in UAV communication networks," *IEEE Commun. Surveys Tuts.*, vol. 18, no. 2, pp. 1123–1152, 2nd Quart., 2016.

[50] S. Hayat, E. Yanmaz, and R. Muzaffar, "Survey on unmanned aerial vehicle networks for civil applications: A communications viewpoint," *IEEE Commun. Surveys Tuts.*, vol. 18, no. 4, pp. 2624–2661, 4th Quart., 2016.

[51] M. Erdelj, E. Natalizio, K. R. Chowdhury, and I. F. Akyildiz, "Help from the sky: Leveraging UAVs for disaster management," *IEEE Pervas. Comput.*, vol. 16, no. 1, pp. 24–32, Jan. 2017.

[52] Y. Zeng, R. Zhang, and T. J. Lim, "Wireless communications with unmanned aerial vehicles: Opportunities and challenges," *IEEE Commun. Mag.*, vol. 54, no. 5, pp. 36–42, May 2016.

[53] T. V. Chien, E. Björnson, E. G. Larsson, and T. A. Le, "Distributed power control in downlink cellular massive MIMO systems," in *Proc. ITG Workshop Smart Antennas (WSA)*, Bochum, Germany, Mar. 2018, pp. 1–7.

[54] P. Chandhar, D. Danev, and E. G. Larsson, "Massive MIMO as enabler for communications with drone swarms," in *Proc. Int. Conf. Unmanned Aircr. Syst. (ICUAS)*, Arlington, VA, USA, Jun. 2016, pp. 347–354.

[55] J. Chen, X. Chen, W. H. Gerstacker, and D. W. K. Ng, "Resource allocation for a massive MIMO relay aided secure communication," *IEEE Trans. Inf. Forensics Security*, vol. 11, no. 8, pp. 1700–1711, Aug. 2016.

[56] Q. Wu, Y. Zeng, and R. Zhang, "Joint trajectory and communication design for multi-UAV enabled wireless networks," *IEEE Trans. Wireless Commun.*, vol. 17, no. 3, pp. 2109–2121, Mar. 2018.

[57] L. Zhang, Q. Fan, and N. Ansari, "3-D drone-base-station placement with in-band full-duplex communications," *IEEE Commun. Lett.*, vol. 22, no. 9, pp. 1902–1905, Sep. 2018.

[58] S. Jeong, O. Simeone, and J. Kang, "Mobile edge computing via a UAV-mounted cloudlet: Optimization of bit allocation and path planning," *IEEE Trans. Veh. Technol.*, vol. 67, no. 3, pp. 2049–2063, Mar. 2018.
[59] H. Yang and T. L. Marzetta, "On existence of power controls for massive MIMO," in *Proc. IEEE Int. Symp. Inf. Theory (ISIT)*, Hong Kong, Jun. 2015, pp.2608–2612.
[60] H. Yang and T. L. Marzetta, "Capacity performance of multicell large-scale antenna systems," in *Proc. 51st Annu. Allerton Conf. Commun., Control, Comput. (Allerton)*, Oct. 2013, pp. 668–675.
[61] T. Van Chien, C. Mollen, and E. Bjornson, "Large-scale-fading decoding in cellular massive MIMO systems with spatially correlated channels," *IEEE Trans. Commun.*, vol. 67, no. 4, pp. 2746–2762, Apr. 2019.
[62] M. Chiang, S. H. Low, A. R. Calderbank, and J. C. Doyle, "Layering as optimization decomposition: A mathematical theory of network architectures," *Proc. IEEE*, vol. 95, no. 1, pp. 255–312, Jan. 2007.
[63] D. P. Palomar and M. Chiang, "A tutorial on decomposition methods for network utility maximization," *IEEE J. Sel. Areas Commun.*, vol. 24, no. 8, pp. 1439–1451, Aug. 2006.
[64] S. Boyd and L. Vandenberghe, *Convex Optimization*. Cambridge, U.K.: Cambridge Univ. Press, 2004.
[65] G. Scutari, F. Facchinei, P. Song, D. P. Palomar, and J.-S. Pang, "Decomposition by partial linearization: Parallel optimization of multi-agent systems," *IEEE Trans. Signal Process.*, vol. 62, no. 3, pp. 641–656, Feb. 2014.
[66] E. L. Lawler and D. E. Wood, "Branch-and-bound methods: A survey," *Oper. Res.*, vol. 14, no. 4, pp. 699–719, Aug. 1966.
[67] H. D. Sherali and W. P. Adams, *A Reformulation-Linearization Technique for Solving Discrete and Continuous Nonconvex Problems*. Boston, MA, USA: Kluwer, 1999.

Zhangyu Guan (Member, IEEE) received the Ph.D. degree in communication and information systems from Shandong University, China, in 2010. He is currently an Assistant Professor with the Department of Electrical Engineering, The State University of New York at Buffalo, where he directs the Wireless Intelligent Networking and Security (WINGS) Lab. His research interests are in network design automation, new spectrum technologies, and wireless network security. He has served as an Area Editor for *Journal of Computer Networks* (Elsevier) since July 2019. He has served as a TPC Chair for the IEEE INFOCOM Workshop on Wireless Communications and Networking in Extreme Environments (WCNEE) 2020, Student Travel Grants Chair for the IEEE Sensor, Mesh, and Ad Hoc Communications and Networks (SECON) from 2019 to 2020, and Information System (EDAS) Chair for the IEEE Consumer Communications Networking Conference (CCNC) 2021. He has also served as a TPC member for the IEEE INFOCOM 2016–2020, the IEEE GLOBECOM 2015–2020, the IEEE MASS 2017–2019, the IEEE IPCCC 2015–2019, and so on.

Nan Cen (Member, IEEE) received the Ph.D. degree in electrical engineering from Northeastern University, Boston, MA, USA, in 2019. She is currently an Assistant Professor with the Department of Computer Science, Missouri University of Science and Technology, Rolla, MO, USA. She directs the Wireless Networks and Intelligent Systems (WNIS) Lab, MST, with research interests in system modeling, control, and prototyping for next-generation intelligent wireless networks.

Tommaso Melodia (Fellow, IEEE) received the Ph.D. degree in electrical and computer engineering from the Georgia Institute of Technology in 2007. He is currently the William Lincoln Smith Professor with the Department of Electrical and Computer Engineering, Northeastern University. He is also the Director of the Institute for the Wireless Internet of Things and the Director of Research for the PAWR Project Office, a public-private partnership that is developing four city-scale platforms for advanced wireless research in USA. His research focuses on modeling, optimization, and experimental evaluation of wireless networked systems, with applications to 5G networks and the Internet of Things, software-defined networking, and body area networks. His research is supported mostly by the U.S. federal agencies, including the National Science Foundation, the Air Force Research Laboratory, the Office of Naval Research, the Army Research Laboratory, and DARPA. He is a Senior Member of the ACM. He is the Editor-in-Chief of *Computer Networks*, and a former Associate Editor of the IEEE TRANSACTIONS ON WIRELESS COMMUNICATIONS, the IEEE TRANSACTIONS ON MOBILE COMPUTING, the IEEE TRANSACTIONS ON MULTIMEDIA, and so on.

Scott M. Pudlewski (Member, IEEE) received the B.S. degree in electrical engineering from the Rochester Institute of Technology, Rochester, NY, in 2008, and the M.S. and Ph.D. degrees in electrical engineering from the University at Buffalo, The State University of New York (SUNY), Buffalo, NY, in 2010 and 2012, respectively. He is currently an Electronics Engineer with the Air Force Research Laboratory, Rome, NY, USA. His main research interests include video transmission and communications, networking in contested tactical networks, convex optimization, and wireless networks in general.